1-1-2013

Improved Limits and Portability Over Currently Employed Cadmium Monitoring Systems Through Preconcentration for Detection by Way of Micro-/Nanofluidic Mechanisms

Paul F. Wach
University of South Carolina - Columbia

IMPROVED LIMITS AND PORTABILITY OVER CURRENTLY EMPLOYED CADMIUM MONITORING SYSTEMS THROUGH PRECONCENTRATION FOR DETECTION BY WAY OF MICRO-/NANOFLUIDIC MECHANISMS

by

Paul Wach

Bachelor of Science
Georgia Institute of Technology, 2009

Submitted in Partial Fulfillment of the Requirements

For the Degree of Master of Science in

Mechanical Engineering

College of Engineering and Computing

University of South Carolina

2013

Accepted by:

Guiren Wang, Director of Thesis

Kevin Huang, Reader

Adrian Mendez-Torres, Reader

Lacy Ford, Vice Provost and Dean of Graduate Studies

ACKNOWLEDGEMENTS

April 1st is a day most use as an opportunity to play jokes on one another. For me it is a day to remember that I am no fool. On April 1st, 2011 I was "let go" from the company I was working for. With no rhyme or reason to the madness unwillingly placed on my shoulders, I could feel the walls crashing in as I drove home. When I arrived at my residence and closed the door behind me, the desire to open the gates of raw emotion was nearly overwhelming. It was at that moment that I took the opportunity to look myself in the mirror. And what I saw was my future. I would not be defeated that day. That bright feeling of warmth, the smile that crept across my face, the sight of a man standing tall brought upon the knowledge that everything would be alright. As I gathered my thoughts, I asked myself the most important question in life. "What would you do if you had nothing holding you back?"

This question, I ask myself often. But my answer that day was to go to graduate school. With this paper, I complete my task. The road was arduous, although not without fun along the way. One thing is for certain, I would not have done this without support. Genetics is the base which creates a limit, but reaching our highest potential is made possible through the nature of nurture. To my family, friends, and God; I say thank you. To my mother and father; you are the base that formed me, the morals that guided me, and the arms that lifted me. To my mentors and colleagues; your wisdom has given me light. To my partners in mischief; you brought the serenity of laughter. To the one who knows and holds my heart; your patience will never be forgotten.

Finally, I would like to acknowledge and thank the members of Dr. Guiren Wang's Microfluidics Lab Fang Yang, Wei Zhao, and Junjie Zhu who helped me struggle through the concepts of micro- and nanofluidics; the members of the Pollocks' Lab and family for their support over the years; Georgia Institute of Technology for providing The life lesson resulting in my understanding of the value of failure and what is means to be a helluva an engineer; University of South Carolina faculty and student body for reminding me that learning should be enjoyable; Savannah River National Laboratory and their scientists Dr. Poh-Sang Lam, Dr. Michael Bronikowski, and Dr. Adrian Mendez-Torres for introducing me to COMSOL with a special thanks to Dr. Mendez for encouraging me to apply to the NNSA Fellowship; Pacific Northwest National Laboratory for their help in getting me the tools needed to finish this project; and the Department of Energy, National Nuclear Security Administration, Ballistic Missile System Acquisitions for awarding me the NNSA Graduate Program Fellowship which has provided funding and time to allow me to complete this research all while learning my new patriotic role for the United States of America.

ABSTRACT

Due to risk of environmental and biological accumulation of Cadmium (Cd), improved methods of early detection and monitoring must be explored as a preventative measure. Listed as one of the top three toxic heavy metals by the Environmental Protection Agency (EPA), the effects on ecological and human systems have well documented side-effects of physical mutation, reproductive sterility, kidney failure, liver disease, bone loss, and death. Found in batteries, metal plating, pigments, plastics, and cigarettes, Cd is also used as a neutron absorber in the nuclear industry as well as having 3 known radioactive isotopes. Urine Cd levels, which have been widely used to predict whole body levels, increase when kidney damage occurs, thus increasing the importance to monitor and detect as early as possible. Although several methods of detection and monitoring are currently in use, they are insufficient for reasons including massive expense, weak specificity causing false readings, and/or a lack of portability. By exploiting naturally occurring mechanisms known to micro-/nanofluidics, a novel approach to Cd detection, measurement, and preconcentration was explored using the finite element computational software COMSOL. An open flow system of a nanochannel was explored through manipulation of the surface charge density. With a dominant negatively charged density on the walls, positive surface charge densities were adjacently placed at the center of the nanochannel causing a constriction of flow and allowing preconcentration of the analytes. When the open flow system was scaled up to a microchannel, the mechanism was found to have little effect on constriction of the flow.

A preconcentration effect was discovered in a closed flow system when the adjacent patches were modeled as being impermeable to charge, causing the molecules to migrate to and remain at the central region of the microchannel once the dynamic process reached steady state. It was found to have the ability to concentrate Cd at an initial concentration of 0.5 mol/m^3, which is nearly half the limit of commercially available technology. Additionally, this preconcentration mechanism was demonstrated to potentially advance its capabilities by attaching channels in series or parallel to further preconcentrate for improved detection. Finally, measurement of extremely low concentrations of Cd is possible due to differences seen in the concentration distribution profiles once steady-state is reached.

TABLE OF CONTENTS

LIST OF FIGURES

CHAPTER 1

INTRODUCTION TO EFFECTS AND DETECTION OF CADMIUM

1.1 SOURCES AND USES OF CADMIUM

Although it can be found in the earth's crust at average levels of 0.18 mg/kg, the main source of Cd in nature is from man-made usage.[1] Typically, Cd is applied during the smelting process of zinc battery manufacturing as well as being used in batteries themselves, such as Ni-Cd batteries. Additionally, Cd coatings are used for steel and copper. Many electronic devices utilize Cd as well; more specifically, in the form of silver solder. Attractive to the ever increasing demand for energy efficiency, another electronic device that makes use of this heavy metal is photovoltaics; where solar cells are fabricated with CdTe. Colors and pigments; especially reds, oranges, and yellows; have been known to be comprised of Cd. Certain plastics, such as Polyvinyl chloride, also contain Cd. The effects of cigarettes and the related suspected carcinogens within them have been widely studied; adding to this is the Cd contents which can be increased through environmental exposure and accumulation on the tobacco plants.[2,3] Bioaccumulation raises concern for meats, especially the liver and kidney since these organs are where the Cd tends to amass. Fertilizers, which are composed of plant and animal bi-products, also have detectable levels of Cd.

1.2 NUCLEAR INDUSTRIAL USE OF CADMIUM

With three known radioisotopes (Cd-109, Cd-113, Cd-113m) combined with the threat of environmental- and bioaccumulation makes Cd a cause of concern for

ecotoxicology, radioecology, and human-health. Argonne National Laboratory has outlined the effects and uses of Cd radionuclides. The half-life of the known radioactive isotopes of Cd are as follows: Cd-109 has a half-life of 1.3 years; Cd-113 has a half-life of 9.3 million years; and Cd-113m has a half-life of 14 billion years. Cd-113m, which emits beta particles with no gamma radiation as it decays, is of the greatest concern.[4] Furthermore, Cd is used as a neutron absorber in the nuclear industry. Behavior of fission products, including Cd, has been studied extensively along with radiochemical determination and systems with liquid-Cd rectifiers.[5-7] Levels of various radioactivity has been monitored since the devastating Fukushima Event, with noted increase in the amount of Cd found in the environment of the United States.[8] Nawrot *et al.* produced a study on environmental exposure of Cd on a population have been performed revealing a connection between environmental exposure to cadmium and cancer.[9]

The threat of environmental- and bio-accumulation raises an increased concern, giving rise to fields of study such as radioecology. Due to time dependent transformation processes such as mobilization of radionuclide species from solid phases or interaction of mobile and reactive radionuclide species with components in solid and sediments; the original distribution of radionuclides deposited in ecosystems will change over time and influence the ecosystem behavior. To access the environmental impact from radionuclide contamination, information on radionuclide species deposited, interactions within the affected ecosystems and the time-dependent distribution of radionuclides species influencing mobility and biological uptake is essential.

1.3 ECOTOXICOLOGY RELATED TO CADMIUM

Effects of Cd to the ecosystem have been well documented from the bottom to the top of the food web.[10-22] Connections have been made from the accumulation of Cd in plants to the effects on humans.[10] Mobility, accumulation, and removal of toxic metals using plants was originally explored by Salt *et al.*, mapping future work from others.[11,12] Gadd *et al.* has more recently reviewed the relationship between fungi and toxic metals, including Cd; finding a relationship between metals and fungi with reference to plant phytotoxicity. Gadd *et al.* takes this a step further, adding that metal-fungal interactions have biotechnological implications for waste removal of toxic metals.[13] Several articles have been written on studies of Cd exposure to the plants, such as a review by Clemens (2001) of metal homeostasis, tolerance, trafficking, transport, and accumulation in plants.[14] Exposure to Cd has been known to cause oxidative stress in plants, with some protection through mycorrhization.[15] Sandalio *et al.* found Cd produces significant changes in the pea plant's growth ability, decrease in transpiration and photosynthesis rate, changes in the root and leaf nutrient consistency.[16] The threat of environmental accumulation of Cd has been observed through the use of the soy bean. Cadmium concentrations as high as 4 times the 0.2 mg/kg limit, established by the Codex Alimenterius Commission, were found despited the soil concentration being well below the maximum allowable Cd concentration. This reinforces the need for Cd concentration monitoring.[17] Metallothionein (MT) bound Cd in the intestinal tract of an insect has been discovered, indicating the influence of diet on Cd exposure.[18] Janssen *et al.* has completed a comparison study between different species of arthropods on the kinetics of Cd, which produced a good predictive model for calculating pollutant flux.[19] Postma *et*

al. varied the levels of Cd in food of *Chironomus riaprius* to study the chronic toxicity effects, revealing a negative effect on larval developmental period and even causing an increase in mortality.[20] Predator-prey interactions have been studied by Riddel *et al.* to observe the response to Cd exposure in an aquatic food web showing a significant effect on the hierarchal response of the energy budgets for individuals and decreased capture efficiency of the predator.[21] Goto *et al.* has also studied the dependence of predator-prey relationship on the transfer of Cd in fish, suggesting that predator fish retained up to 11.0% of Cd found in their prey.[22] Much of the Cd will be retained by the fish and accumulated over time.

Due to their semi-permeable skin, amphibians are of particular interest when studying Cd absorption and kinetics. The Ecologist Ravera, would agree on the importance of studying metal speciation in an aquatic ecosystem and point to the difficulty in carrying out such studies.[23] A review of the effects of Cd on amphibians has been performed by Gross *et al.* revealing negative effects on the growth and development of tadpoles.[24] Cd exposure has been found to have sex differentiating effects as well as causing changes in metamorphosis.[25] Jame et al (2x) observed the hibernation cycle of toads when introduced to Cd as well as the metamorphic results to chronic Cd exposure. These results revealed only a 56% survival rate of toads fed worms with 4.7 ug Cd per g body weight versus 100% survival rate of the controls in one study, which was found in agreement with other studies on changes in metamorphisis.[26,27] Toxic and genotoxic potential of Cd, more specifically $CdCl_2$ which is a water soluble compound, has been evaluated by Mouchet *et al.* and found to have acute genotoxicity of 2 mg Cd/L one species of amphibian larvae while being genotoxic at all concentrations for another

species.[28] Fridman *et al.* introduced Cd to amphibian embryos to study uptake, toxicity and metabolism effects; suggesting that Cd exposure causes a disruption in the endocrine system.[29] Industrially developed areas in close proximity to wetlands have documented Cd concentration levels as high as 703 ug/L and an average water concentration of 1.0 ug/L in the United States, leading to the altered growth patterns seen in amphibious life through chronic, low dose exposure to Cd.[30-33] An influence of Cd on the thyroid hormone (TH) has been suggested after studying the effects on frog growth cycle.[24] Of importance to note, is the difference in results of Cd exposure on amphibians based on the route of exposure, whether it was absorbed through the gills and skin or through the gastrointestinal tract after consumption, suggesting that both lead to harmful bioaccumulation.[27,34]

1.4 EFFECTS OF CADMIUM ON HUMANS

The human kinetics of Cd initially depends on the intake method; however, the end result is similar. Although minimal, Cd can be absorbed through the skin by binding to MT and transported through the blood stream. When ingested through the gastrointestinal tract, Cd can be absorbed in several different ways; such as metal transport complex or endocytosis of proteins. What Cd is not excreted through feces is absorbed into the blood stream. The lungs function to transport oxygen and other valuable nutrients directly into to the blood stream. Due to the direct path to the blood stream, unblocked inhaled toxins can have series health implications. In the form of Cd-Cysteine, cadmium is absorbed directly into the blood stream. Once in the blood stream, Cd is transported with MT, glutathione, cysteine, and proteins to complex. From the blood, Cd travels to the liver where Cd-MT is synthesized. Cadmium is then stored as

Cd-Glutathione, Cd-Cysteine, Cd-MT, and Cd-Protein. There are two pathways in which Cd can reenter the blood stream. The first is conjugation with glutathione, where it is then secreted via the biliary system. The second occurs after hepatocyte necrosis or apoptosis, causing Cd-MT to be released back into the blood stream. The Cd compounds then travel to the kidney where it is stored in complex as Cd-MT or Cd-Protein. Cadmium is then excreted very slowly and in small quantities through the urine. For more detailed explanation of the Cd kinetics in the human body see Godt *et al.*[35]

Research has been well documented on the effect of Cd exposure on the human population.[36-41] To the public eye, perhaps the most notable potential effect of Cd exposure is its carcinogenic effect.[9,42-44] The International Agency for research on Cancer (IARC) has placed Cd in category 1 of carcinogens.[43] Nawrat *et al.* have performed a study on a population analyzing patients with cancers, connecting Cd exposure as having a significant risk association.[9] Since tobacco is a plant and cigarettes are a known carcinogen, it is important to analyze the potential uptake of Cd into the tobacco plants and transfer into humans. Such studies have been performed by Nnorom *et al.* & Martin *et al.*[42,44] Toxicokinteic modeling is important for use as a risk assessment tool. Amzal *et al.* has assesses the health risks of Cd using a population toxicokinetic model, estimating the half-life of Cd to be approximately 11.6 years.[45] Vallee *et al.* have written a detailed biochemical analysis of Cd effects throughout biological systems, including reviewing enzymatic activities that are enhanced by Cd.[38] Genomic instability as a result of Cd exposure and its mechanism has been explored by Filipic, suggesting that low concentrations of Cd can produce genomic instability in non-occupationally exposed humans.[46] The genotoxic effects include interference with DNA

repair, damaged signaling processes, apoptotic pathways; oxidative stress induced through mitochondrial exhalation of reactive oxygen species (ROS) and depletion of cellular antioxidants.[39-41,46-49]

Due to the toxicity of Cd, the United States government has placed several regulations on release of Cd into the environment and allowable exposure of workers deemed the "risk population". As per the Safe Drinking Water Act of 1974, the EPA is required to establish the Maximum Contaminant Level Goals (MCLG), after which a Maximum Contaminant Level (MCL) is set at or very close to the MCLG. In most cases these values are established to be the same, which is the case for Cd as set at 5 parts per billion.[50-52] It is important to note the difference in solubility of Cd compounds. According to the EPA, while cadmium oxide (CdO) is insoluble in water, other Cd compounds may be highly soluble; such as cadmium chloride ($CdCl_2$) which has a solubility in water of 14 g/L at the low temperature of 20 ^{o}C. The Occupational Safety and Health Administration (OSHA) has regulations listed for each industry relating to Cd from agriculture (1928.1027), shipyards (1928.1027), construction (1926.63), to general industry requirements (1910.1027). Where potential exposure to toxic materials is possible, OSHA is charged with the task of determining the Permissible Exposure Limit (PEL). For the high "risk population" of the workers in Cd related industries, OSHA has set the PEL at 5 ug/m^3 over a period of 8 hours.[53-56] Inhalation of toxic substances has a significantly different response, which in most cases will expatiate the reaction. Histopathology of Cd in the liver and lungs has been observed in frogs by Ikechukwu *et al.*,[57] which confirms concern for Cd exposure in the form of inhalation for humans. As a result, OSHA sets a limit on the amount a substance can be released into the air, or the

Separate Engineering Control Airborne Limits (SECALS). For Cd, the SECALS ranges from 15-50 ug/m^3 depending on the industry. Furthermore, OSHA has an Action Level (AL) at which employers are required to perform exposure monitoring and medical surveillance. Once the exposure over the AL is reached, which is 2.5 ug/m^3 for Cd, monitoring is required every six months.[53-56]

As previously mentioned, notable differences can be observed through the different pathways of intake and dose responses of Cd exposure. There is a 10 fold increase in toxicity of Cd ingested over a short-term period versus long-term exposure. Similarly, inhalation has a 100 fold increase of toxicity in short-term versus long-term exposure of Cd.[52] Typical acute responses to Cd exposure involve flue like symptoms with stomach irritation, vomiting, and diarrhea; although, higher doses may cause injuries to the testes, liver, lungs, and potentially death.[52,58,59] Higher risk is seen in chronic low dose exposure to Cd; which can cause permanent damage to areas such as the testes and lungs, emphysema, pulmonary disease, bone loss, immune-suppression, liver disease, end stage renal disease (ESRD), and death. [36,52,61,62] The kidney is specifically important to the body's ability to clean the blood, impairment of this function can result in significant cardio vascular issues.[63,64] Once in the body, Cd will travel through the blood stream and settle in the liver and kidney. Cd induces proteinuria, leading to impaired renal function and osteomalacia.[65,66] Once entered into the blood stream, Cd accumulates in the lymphocytes where it binds to MT and transports the Cd to the liver and kidney.[67-71] As an intracellular scavenger, MT provides protection for Cd, increasing its accumulation in the body and leading to a long half-life.[67-69,72] Due to the binding of MT to Cd, measurements of this biomarker are often used to measure Cd levels in the body as

excreted through the urine.[73,74] Although, Cd can be detected in the blood stream, urine Cd level may be a better predictor of toxicity. When renal damage occurs, urine Cd levels increase thus making the need for consistent monitoring a necessity.

1.5 CURRENT CADMIUM DETECTION AND MEASUREMENT METHODS

According to the International Program on Chemical Safety, it is recommended that samples must be taken as a "static" air sample from the workplace as well as a "personal" sample for Cd level measurements; which is outlined as a part of Environmental Health Criteria 134. The personal sample is often much higher than the workplace sample which is frequently an underestimation; making the personal sample a better indicator of Cd levels. Even with recent development in technology that requires less sample size in the range of mL or g of biological samples, there is currently no method that provides the concentration of Cd with one hundred percent precision. The closest to a "true" concentration of Cd is given through isotope dilution mass spectrometry (IDMS); however, this requires an "ultraclean" facility and is extremely expensive. Several other methods exist for measuring Cd levels; including atomic fluorescence spectrometry, colorimetry with dithiozone, and proton-induced X-ray emissions (PIXE) analysis. Although, the most commonly used methods for Cd measurements are (1) atomic absorption spectrometry, (2) electrochemical methods, and (3) neutron activation analysis.[75]

Atomic absorption spectrometry: Atomic absorption spectrometry is the most commonly used method, which involves passing the sample through a burner at high-temperature and measuring the absorption of the heat from the ground state atoms. This method has been used to determine Cd concentrations in water,[76,77] biological materials

such as human hair,[78,79] and urine.[80] The detection limit for this type of method is 1-5 mg/L of pure water and 0.1 mg/kg of biological samples.[75] Some enhanced methods have been explored, such as electrothermal atomization (ETA). This method of atomizing samples requires increase sensitivity, usually by preconcentration, and 1-100 mL for sample testing.[75] ETA has a lower detectable limit of Cd concentration in blood and urine of 0.1-0.3 mg/L.[81] Although this is the most widely practiced method of measuring Cd, there is significant issue with light scattering as, such as caused by phosphate ions, a result of particle and nonspecific absorption as a result of broad molecular absorption bands. For example, a 0.5 mg/L concentration of sodium chloride produced a signal corresponding to 0.2 mg of Cd/L when the actual concentration of Cd was 0.4 mg/L.[82] The necessary background correction, sample size, and the need for preconcentration are three flaws that should be improved.

Electrochemical methods: The basic principle behind electrochemical methods revolves around measuring the electrochemical potential created as electrons transfer between metals. Recent development in technology has made use of anodic stripping voltammetry in which previously reduced metals are released and bound to the mercury electrodes. As one of the methods of Cd detection with the most sensitivity, a peak current is measured at a specific potential to the metal under analysis. The detection limit for this method is approximately 0.1 mg/L of urine.[83] Although there are Cd-selective specific electrodes commercially available, they lack the sensitivity required for measurement of biological materials.

Neutron activation analysis: Activation analysis is used to create radioactive Cd isotopes through irradiation with neutrons, which is then measured by recording the

specific energy and half-life of the specific isotope. Neutron activation analysis has been used in the past to measure Cd in human liver.[84] One drawback to this method is the potential requirement to concentrate Cd and separate is from other isotopes present that have overlapping energy spectrum. For most biological samples, the detection limit is 0.1-1 mg of Cd/kg or 0.1-1 mg/L for neutron activation analysis.[75] This method is often only used in screening programs as a result of the large expense involving the use of a reactor for the irradiation process. In many cases, this method is used as a reference for accuracy when testing other methods.[85-87] One major disadvantage to this method is the potential for liquid samples to explode as gases are forms during the irradiation process, making this method ineffective for measuring Cd levels in urine or blood samples.[75]

There are some *in-vivo* methods for determining Cd levels in the liver and kidney.[88-90] Through utilizing the naturally-occurring Cd-133 isotope and the large capture cross-section, neutron activation can be performed on whole organs. A portable unit has been developed with a Pu238-Be source of neutrons.[91] As a "field" unit, this method has the lowest detection limit of 1.5 mg/kg of liver and 15 mg/kg of kidney.[92] This method has some variability based on the location of the kidney and needs further development.[93] Using X-ray generated atomic fluorescence, Cd levels can be detected in the kidney cortex.[94,95] The detection limit for this method has been determined to be 17 ug/g of kidney cortex;[96] and although this number is low, the precision is only 23 percent.[75] The detection limits and technology is important to note; however, the lack of applicability to liquid samples, makes this technology irrelevant to the end target of this research paper.

1.6 PROPOSED IMPROVED TECHNOLOGICAL RESPONSE

With the current methods of Cd detection either extremely expensive, large sample size requirements, giving false values, insufficient sensitivity, and/or having problems with liquid samples; a new technology for Cd monitoring must be implemented as a preventative measure to combat environmental and biological accumulation of Cd. Utilizing the principals of nature in the form of micro- & nanofluidics offers a unique approach to solving the issues relating to Cd detection with low sample size requirements in the range of uL to pL; low cost due to low material consumption; point-of-care methodology and instrumentation, such as Lab-on-a-Chip (LOC) technologies; and significantly improved specificity and selectivity made possible through the effects of having a low Reynolds number.[102-103]

Recent efforts in micro- & nanofluidics have focused on such issues as DNA analysis, first used by Han *et al*.[97] With the device arranged in a repeating series of one microchannel followed by a nanochannel, single strand DNA analysis is made possible. The implications of this are high throughput in detection of biomarkers for diseases and cancers, which can be integrated with micro-total analysis systems (μTAS). Entire organs are being modeled and developed using micro- & nanofluidics, such as the human nephron filter created as a means to miniaturize renal replacement therapies for portable implantable and/or wearable artificial kidneys (WAK).[98] A discovery of ion governed transport in microfluidics, which has potential for use in Cd detection, was made by Stein *et al.* at the Kavli Institute of Nanoscience.[99] Although this surface charged governed ion transport is useful for separation and filtration processes, more is required to create an effective Cd monitor.

The application of microfluidics in relation to cadmium is relatively new, occurring within the last year. Cadmium selenide, which is used as a semiconductor, was synthesized using microfluidic mechanisms as part of a thesis dissertation at California Polytechnic State University.[111] Another study was performed to analyze the cytotoxic effects of Cd, which was slowly introduced to fibroblast cells and found to suggest apoptotic pathways were behind cell death.[112] A recent experimental technique for microfluidic fluorescent detection has been studied and was found to have a detection limit of 0.45 ug/L.[113] Although this has a rather low limit, the detection range only needs to at or slightly below the established monitoring limits of 5-2.5 mg/L.[53-56] Furthermore, this technique described in this paper would require a complex system consisting of a computer, frequency generator, power supply, and amplifier. The goal of the study below is to develop a monitoring system such that Cd detection can be performed in the field with the human eye.

The unique and potential for mobility make detection, measurement, and preconcentration options that should be explored for application of in-field detection of Cd. When liquid is contacted to a dielectric surface, there is a thin electric double layer (EDL) near the surface. In a nanochannel, due to the overlapping electric double layer (EDL), a preconcentration effect can be seen at the micro- to nano-interface when a driving force is applied through either a voltage or hydrodynamics.[100] The results of the voltage driven and hydrodynamic driven flows vary the preconcentration effect and should both be explored for this application. However, there is concern for potential clotting from larger than nanoscale particulates at the nanochannel interface, which can potentially be overcome through the use of similarly charged electrode placed at the

desired concentration point that will extend the EDL and in effect replicate the desired nanochannel filtration effect. With the most widely used method of atomic absorption spectrometry for measuring requiring preconcentration,[75-82] the use of micro-/nanofluidic offers the ability to measure the concentration at the same time as preconcentration and detection of Cd.

CHAPTER 2

METHODICAL PROCESS TO SIMULATION

2.1 OPEN FLOW SYSTEM NANOCHANNEL PRECOCENTRATION

The conceptual idea presented in this paper is designed to overcome the restrictions based on traditional nanofluidic devices that tend to clot. The original simulation was based on a model problem provided by COMSOL commercial software of a nanofluidic mixture; in which a surface charge density (σ) of -0.02 C/m^2 was placed on the walls of a 10x60 nm^2 channel. The mixing created in a nanochannel through placing positively charged patches of 0.06 C/m^2, 20 nm apartment and on opposite walls of the channel. The simulation contained two particles of opposite charge with a valence of +/-2. The two particles were treated as equal for all other parameters, with diffusivity and concentration being the parameters specific to the analytes. A temperature of 300K was used for the experiment. A voltage of 6e-7 V was applied to the left opening of the channel and was used to drive the flow from left to right through electroosmosis. The question was asked of how the flow would react if the positively charged patches were moved to the center of the channel directly opposite of each other. It was suspected that an alteration of the conditions could cause a bottle neck of the flow by changing the positions of the positive surface charge densities to the center walls of the channel directly opposite of each other and as a result create a preconcentration effect. (FIGURE 2.1)

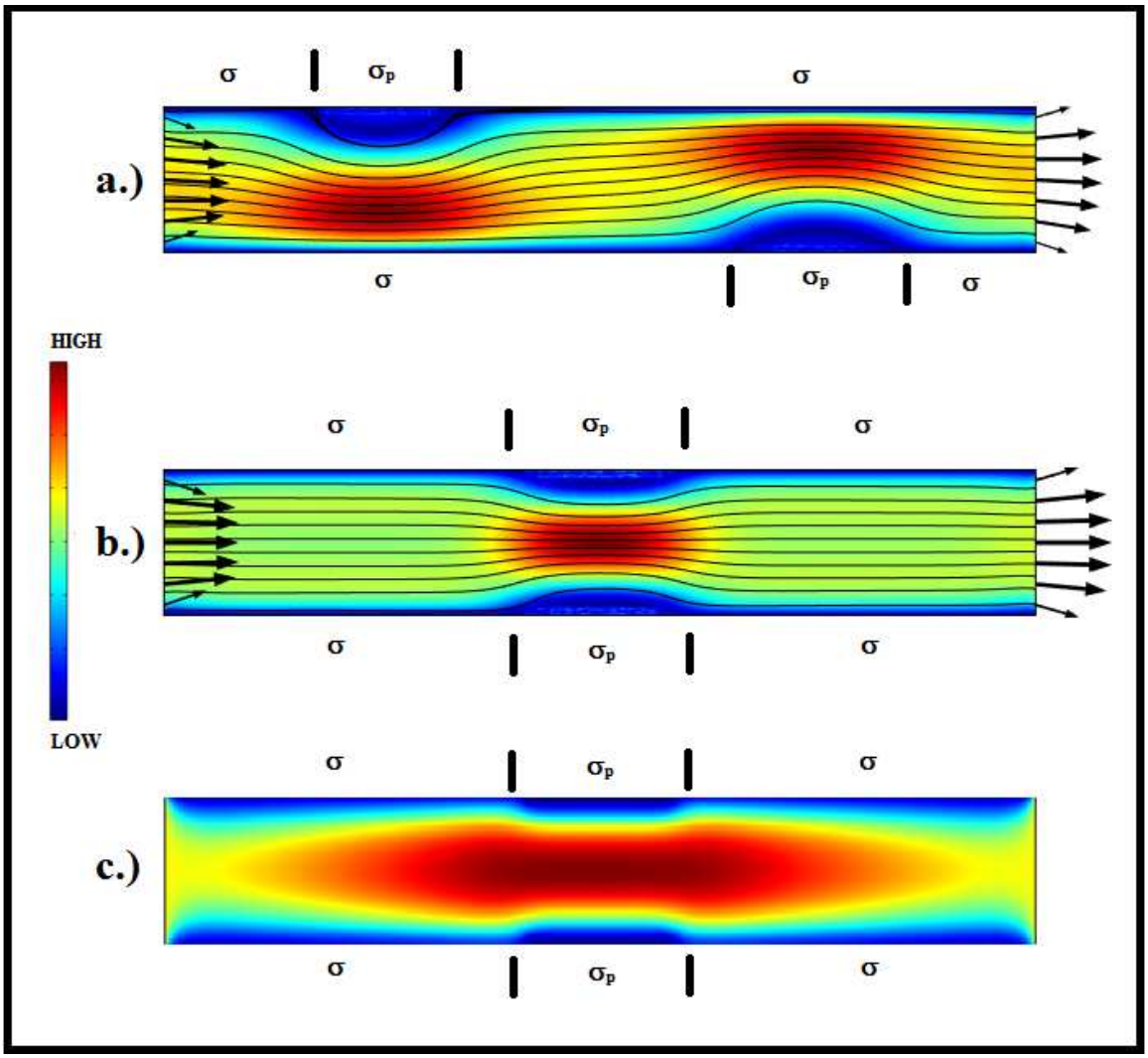

Figure 2.1 Nanochannel Mixer and Preconcentration: All are nanochannel with dimensions 10x60 nm^2, the color scheme represents the intensity where RED is high and BLUE is low, the BLACK lines and arrows represent the flow profile and direction, σ is the negative surface charge density, and σ_p is the positive surface charge density; a.) is a nanochannel mixer where σ equals -0.02 C/m^2 and σ_p equals 0.06 C/m^2; b.) Velocity profile of a nanochannel preconcentration where the red is the highest velocity, blue is the lowest velocity, the black arrows are the direction of flow, the black lines are the stream lines of the particles, σ equals -0.02 C/m^2 and σ_p equals 0.06 C/m^2; c.) is the concentration profile of nanochannel preconcentration where the highest concentration (RED) can be seen at the center, lowest concentration (BLUE) can be seen at the outer edges, σ equals 0.02 C/m^2, and σ_p equals 0.2 C/m^2.

This did in fact cause a constriction of flow at the center of the channel where the positive patches were located as can been seen in the difference between a.) and b.) in FIGURE 2.1. As can be seen in this figure, the flow in a.) was redirected when approaching the walls with a positive surface charge density. This concept was taken a step further by moving the positive patches to the center of the channel causing the flow to constrict at this region. Although the flow was constricted at this central region shown in Figure 2.1b, the positive analyte was drawn to and largely stayed at the surface where the charge was negative. To overcome this, the surface charges were made to be positive and increased in magnitude. The results of this, shown in the concentration profile Figure 2.1c, revealed that the positively charged particles no longer stuck to the walls and displayed a constricted flow at the center of the channel. In Figure 2.1c, the RED color represents the highest concentration and the blue denotes the lowest concentration. This is also applicable to the entire thesis. If this is possible at the nanoscale, it was speculated that a similar results could be seen and utilized at the microscale, which would be beneficial to prevent clotting seen in nanofluidic devices.

2.2 OPEN FLOW SYSTEM MICROCHANNEL PRECONCENTRATION

The next step was to increase the scale to micrometers to then simulate the same effect seen as nanofluidic preconcentration; however, despite significant effort, this concept proved to be unsuccessful. Based on several variations in the simulation, the same level of flow constriction was not able to be seen on the microscale as on the nanoscale. Using the original surface charge densities and a proportional voltage driven flow, the constriction of flow at the center of the channel was insignificant. Increasing the surface charge density 1,000 fold, proportional to the increase in channel size, proved

to created complication in the computation of the electric field gradient and was therefore deemed an ineffective method.

Additionally, a voltage was used on the surface walls in an attempt to create a proportional electric field. Since electrodes have an inherent electromagnetic field, it seemed plausible that placing electrodes of the same charge along the surface wall would serve to replicate the effect of the surface charge density and further open the door to controlling the preconcentration method. Using the electric field calculated by the software created by the surface charge density, the voltage needed to produce a similar electric field was reverse calculated and used for these simulations. First attempts saw issues with the electric field gradient once again. As a result the model was simplified to create a proportional electric field as seen in the nanopreconcentration model. (FIGURE 2.2) In FIGURE 2.2a, the electric field distribution and intensity was modeled without including the transport of dilutes species and laminar flow modules in order to calculate the voltage needed to create a proportional electric field distribution in a microchannel. As seen below, the intensity of the color scheme for the electric field distribution is proportional and in same direction as per the white arrows.

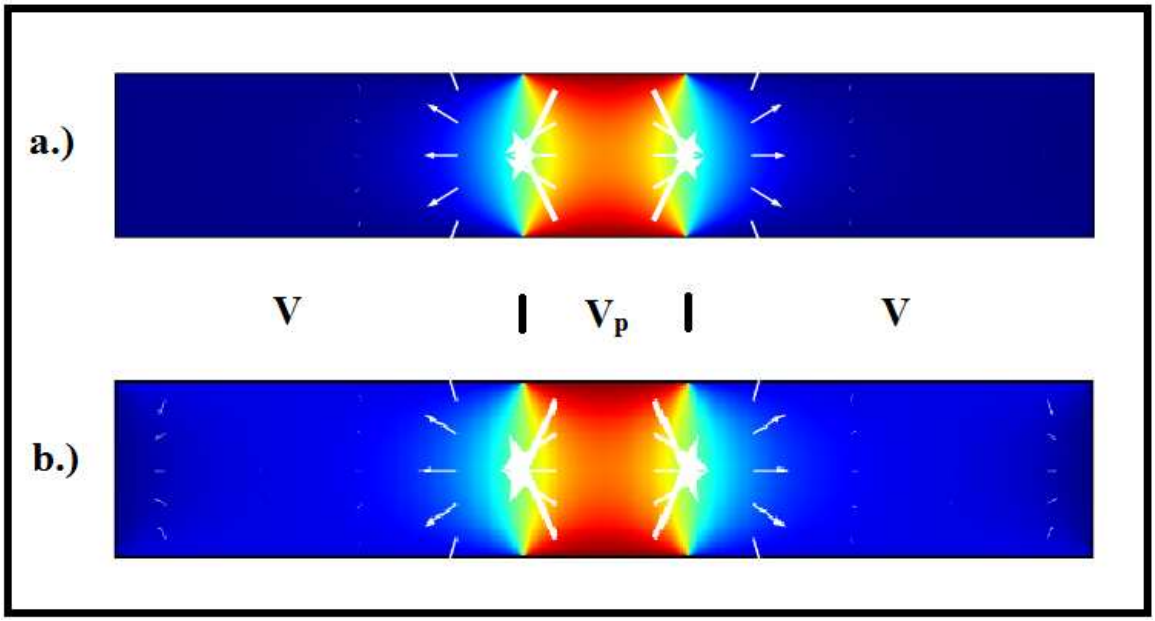

Figure 2.2 Upscale of Electric Field from Nano- to Microscale: Electric field distribution where RED is the highest intensity, BLUE is the lowest intensity, the WHITE arrows are the direction of the electric field, V is the lower positive voltage used to replicate a surface charge density, V_p is the higher positive voltage used to replicate a surface charge density, a.) is a nanochannel, and b.) is a microchannel.

It was speculated that this would then cause the pinch in flow profile previously seen; however, this was not the case. The simulation revealed that the analyte was either prevented from flow through the channel or passed through with zero change in profile. Adjustments were made to both the voltage driven flow and the voltages placed along the surface of the wall with no significant changes. It was then speculated that perhaps adding a ground point at the center of the channel would cause a flow toward that central point; however, the analytes traveled beyond the ground point with no change in flow profile. Additionally, the voltage driving the flow was also studied. Decreasing the driving voltage would cause an increased change in flow; however, if this voltage were to no longer be present and the system was changed to a closed system, the analytes would then travel to and settle at the surface with the opposite charge of the analyte at

equilibrium state. Since this was not the original intent of the study as this would take a length of time to reach steady state and would also lose novelty of the concept, it was ignored.

2.3 BASE MODEL: CLOSED SYSTEM PRECONCENTRATION AND DETECTION

The focus of the original study was not only to achieve preconcentration but also to have rapid detection to be used in field application. The system was then simplified to a closed system and the question was then asked of how the simulation would react if the preconcentration voltage, and/or surface charge density at the center walls of the channel, was removed entirely. An interesting result was observed during initial simulation, the analytes congregated at the center of the channel. (FIGURE 2.3) FIGURE 2.3a shows that the intensity of the electric potential is highest at the center, where there is no charge at the channel walls. FIGURE 2.3b reveals that the bulk flow is toward the center of the channel. Additionally, any molecules that escape the bulk flow are circulated along the wall, pushed away from the center, and then enter the bulk flow once reaching the left and right sides of the channel. All molecules are eventually trapped at the center of the channel as seen in FIGURE 2.3c, where the highest intensity of the concentration is in RED. A time-dependent simulation was run, which confirmed the flow pattern and trapping of molecules at the central region of the channel. Additionally, this process occurred nearly instantaneously, happening between 1-2 seconds. Effectively, the mechanism found here acts to preconcentrate the molecule, making it possible to detect at low concentrations of analytes. This phenomenon was then explored in-depth.

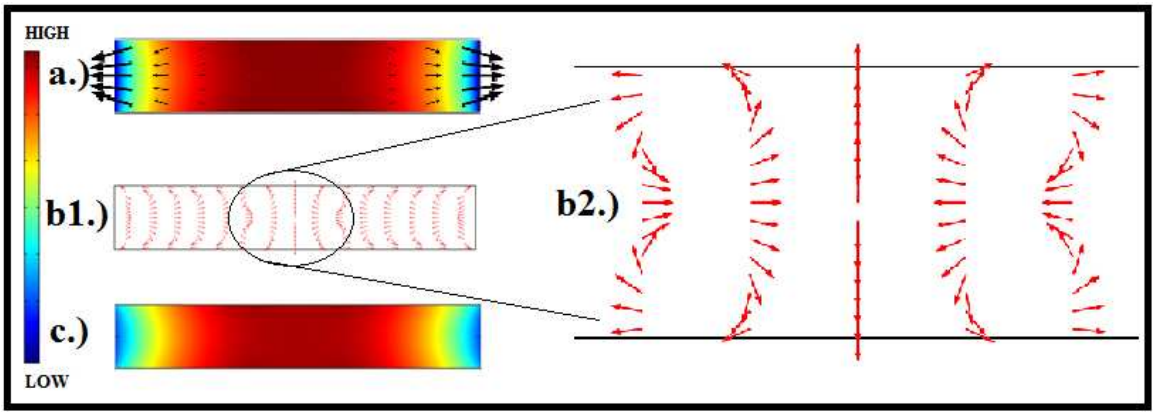

Figure 2.3 Closed System Microchannel Preconcentration: a.) electric potential distribution, RED high potential, BLUE low potential, BLACK arrows are the direction of the electric field with the smaller arrows at the center representing a smaller gradient and the larger arrows at the outer edges representing a larger gradient; b.) flow velocity profile where the RED ARROWS represent the direction and proportional magnitude of the flow; c.) concentration profile of the negative analyte with the highest intensity in dark RED at the center of the channel where the walls were uncharged.

2.4 COMPUTATIONAL APPROACH

Software: Initial simulations were under steady state conditions, meaning all of the inputs were spontaneously applied and the end result was calculated with COMSOL finite element analysis software. Initial experiments were run using COMSOL version 4.3. The majority of simulations were run using COMSOL version 4.3a and final computations were completed with COMSOL version 4.3b.

Geometry of the micro-preconcentrator: The model was a two-dimensional slice of a channel with a 10 μm height (y-direction) and 60 μm length (x-direction). (FIGURE 2.4) A voltage specified as *V0* was applied to the left side of the channel, wall 1, and an electrical ground placed to the right side of the channel, wall 8, creating a DC voltage used as the driving force. A surface charge density was applied to the walls 2, 3, 6, and 7, which were 25 μm in length. On surfaces 4 and 5, there was zero charge on these 10

um patches. It is between these two patches that the largest concentrations were found to accumulate as a result of the applied conditions.

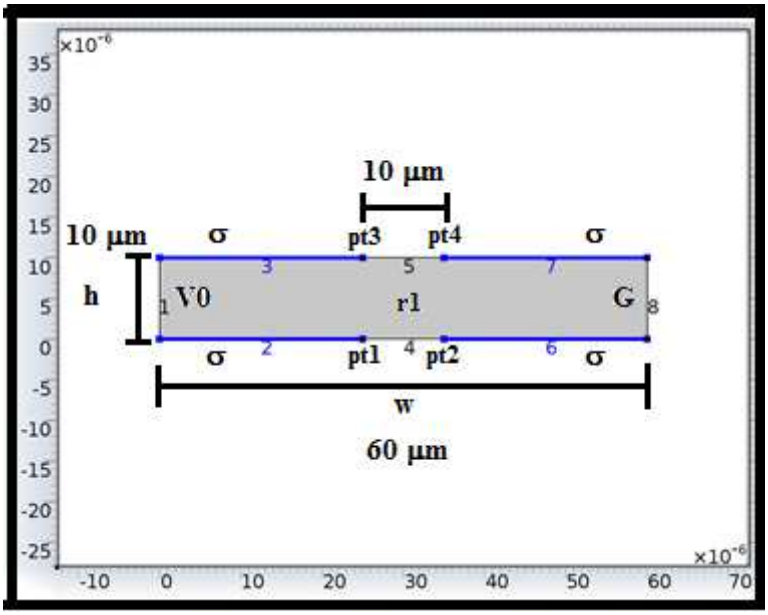

Figure 2.4 Dimensional and Variable Explanation: 10x60 um 2-D slice of a microchannel where *r1* is the domain contained by boundaries 1-8 in which the fluid is contained; *pt1*, *pt2*, *pt3*, and *pt4* represent the points of transition from the surfaces with a charge density and surfaces without a surface charge density; *V0* is the applied voltage; σ is the surface charge density on walls 2, 3, 6, and 7 (BLUE); walls 4 and 5 are the uncharged surfaces; and *G* represents the surface modeled as an electrical ground at surface 8. The x-axis and y-axis represents distance in µm.

In order to create a simple model to better understand the results, the same values were applied to arbitrary molecules; each had the same diffusivity, concentration, and opposite valence. The mobility was calculated using the temperature (300K) and the universal gas constant (8.314 J/mol-K). In the case of modeling microfluidics it is usually assumed that water is filling the channel and therefore the properties of water provided a relative permittivity of 80, density of 1e3 kg/m^3, and dynamic viscosity of 1e-3 Pa-s was used. The model required 3-way coupling of electrostatics, laminar flow, and transport of diluted species. It should be noted that a 3-way coupling significantly increased the computational demand and may have been the cause of much of the

problems in previous simulations, which was in part the reason for simplification of the model to a closed flow system.

Equations: Using the Electrostatics module, the voltage driven flow was modeled. Additionally, this module was used to set the conditions for the surface voltages and surface charge densities. With these applied conditions, the electric field was modeled. Charge conservation across the channel was calculated using quadratic discretization through the equations below;

$$E = -\nabla V \quad (1)$$

$$\nabla \cdot \varepsilon_0 \varepsilon_r E = \rho_r \quad (2)$$

where *E* is the electric field, which equal the gradient of the voltage (V), and the gradient of the permittivity constant ε_o times the relative permittivity ε_r time *E* equal to the relative space electric charge density ρ_r. Material type was non-solid since water is modeled as filling the channel. Zero charge condition was placed at boundary 4 and 5. (FIGURE 2.4). Note this means that zero permeability of charge through the surface; which is not to be confused with pacing a ground at these boundaries, an option that was tested and did not produce the same results. An initial voltage of zero was applied to the entire domain, which means that a dynamic process occurred until the simulation reached steady state. An electric potential was applied at boundary 1, represented by *V0,* at a value of 6e-4 V with a ground placed at the opposite boundary 8, represented as *G,* to drive the flow from left to right. A surface charge density represented as σ at a value of -0.02 C/m^2 was set at boundaries 2, 3, 6, and 7. The space charge density of the domain was calculated by adding the products of the valence and concentration of each analyte and multiplying by body force.

$$\rho_r = F(z_1 c_1 + z_2 c_2) \tag{3}$$

where ρ_r is the relative space charge density, F is body force, z is the valence of the of each species of molecule, and c is the concentration of each species of molecule in the solution.

In microfluidics the fluid is assumed to be laminar since the Reynolds Number is on the order of 1.[102,103] Additionally, it is generally treated at incompressible as was the case in this model. Also, there must be a conservation of mass. The following equations were used to approximate the flow of the analytes using quadratic discretization. The non-slip boundary condition was applied to all boundaries as this is a closed system, meaning the velocity is zero at the walls.

$$u = 0 \tag{4}$$

where u is the velocity of the fluid. In microfluidics it is always assumed that velocity at the wall of a pipe/channel is zero due to friction. However, in micro- and nanofluidics, this friction is speculated to not exist due to a sliding of charged particles created by their inherent electric field. For simplification purposes of this study, this theory is ignored. Mass conservation is calculated using the continuity equation;

$$\frac{\partial \rho}{\partial t} + \nabla \cdot (\rho \vec{u}) = 0 \tag{5}$$

where ρ is the density, t is time, u is the vector velocity of the fluid. This means that the mass contained in the channel will not change. For incompressible flow, since mas must be conserved and the density of the material does not change, therefore;

$$\nabla \cdot \vec{u} = 0 \tag{6}$$

where u is the vector velocity of the fluid. Momentum must also be conserved and was calculated using Navier-Stokes Equation;

$$\rho\left(\frac{\partial \vec{u}}{\partial t} + \vec{u} \cdot \nabla \vec{u}\right) = -\nabla \rho + \mu \nabla^2 \vec{u} + \vec{F} \quad (7)$$

where ρ is the density of the fluid, *u* is the velocity of the fluid, *t* is time, and *F* is body force. Since ρ and *u* are both independent known variables, these series of equations are used to calculate the body force, *F*. This is then used to calculate the relative space charge density, ρ_r, from the Electrostatic module. Since the relative permittivity ε_r and permittivity constant ε_o are both known values, the electric field *E* can be derived as well as the final voltage values across the channel. Initial values of velocity in the x and y directions were set zero m/s; although it was discussed to be an option to create and initial Brownian Motion; however, this was determined to not affect the final result based on preliminary studies. Pressure was set at zero Pa. It should be noted that the option of using hydrodynamic driven flow as opposed to voltage driven was discussed and studied; however, was later determined to not be a viable option as this would eliminate the concentration of the positive analyte at the center of the channel. Initially, a pressure value of zero Pa was specified at Point 2 to reflect a closed system (FIGURE 2.5) A pressure point of zero was specified at each corner of the channel (points 1, 2, 7, and 8) was later used to create better symmetry and therefore a more realistic closed system.

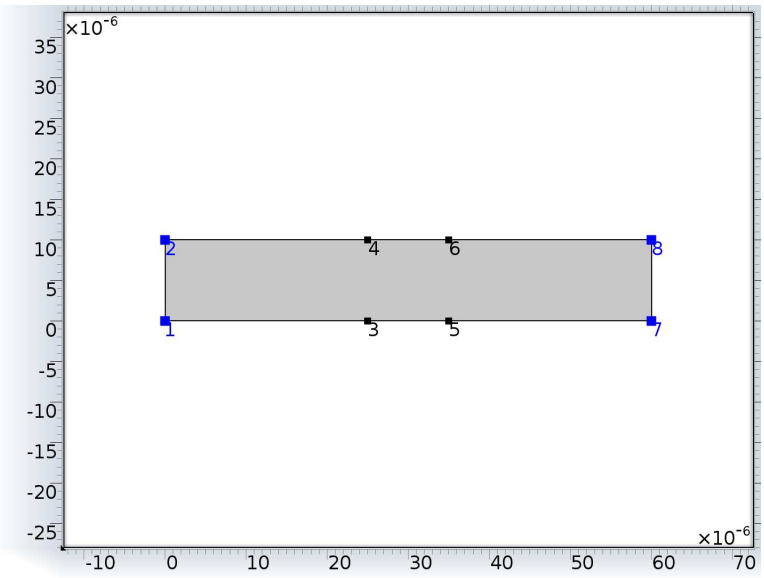

Figure 2.5 Dimensional Pressure Point Explanation BLUE squares represent the locations of pressure point constraint used to create a symmetrical closed system. The x-axis and y-axis represents distance in μm.

The Chemical Species Transport model was used to simulate the transport mechanisms of convection and migration in an electric field. Quadratic discretization was used to calculate the final concentrations of the analytes. The velocity field, *u*, was calculated by the software under the conditions of creeping/laminar flow and single phase, meaning that transport was dependent on both the electrostatics and flow. The electric potential (*V*) was input through coupling this model with the previous Electrostatic model. No Flux condition was applied to surfaces 2-7. An initial value of a uniform concentration as previously specified (10 mol/m^3) was set across the entire domain as well as at boundaries 1 and 8 to set the system up to potentially change to an open system. Quadratic discretization was then used to reverse calculate the final concentrations of the analytes and there approximate distribution across the channel.

Mesh: The finite element mesh was user defined and calibrated based on optimization for fluid dynamics. Due to the application of the non-slip conditions the

velocity gradient between the wall and the center of the channel is quite large. Additionally the difference between the bulk flow and flow at the wall should be calculated using a different mesh, since the velocity gradient is larger near the wall. As a result the mesh size was much smaller at the wall and a growth factor of 1.15 was used as the mesh increase from flow at the wall to bulk flow. Corner refinement, free triangular, and boundary layer properties were defined to help define the mesh and create a smooth transition to from the wall to the center of the channel. The complete mesh consists of 15,014 triangular domain elements and 504 quadrilateral boundary elements and contained 186,885 degrees of freedom. (See FIGURE 2.6)

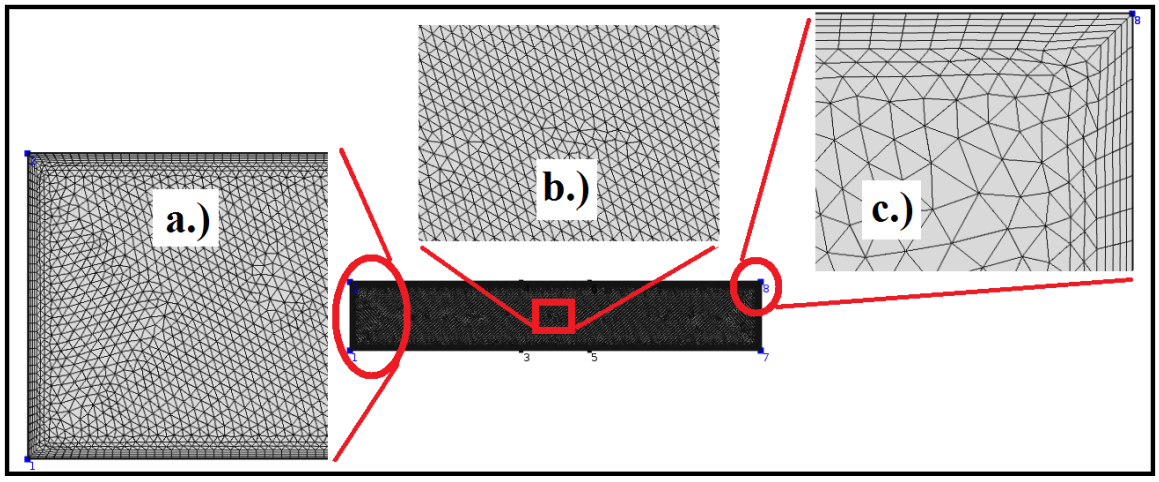

Figure 2.6 Finite Element Mesh: Finite element mesh with 5 layers quadrilateral boundary elements at the walls and a specified growth factor to help transition from the quadralateral to the triangular domain elements that make up the bulk of the 2-D model where a.) is shows the elements at the left boundary, b.) shows the triangular elements at the center of the channel, and c.) shows the transition from quadrilateral to traingualr elements at the upper right corner.

Three studies were performed in each simulation. The first was simply to model the electric field created by the Electrostatic module. The second study was to couple the three modules Electrostatic, Transport of Diluted Species, and Laminar Flow. The

third was to develop a time-dependent model with all three modules combined in order to determine the length of time require to reach steady state.

Electrostatic modeling: This was to assure that the electric field was realistic and would not cause an unreasonable demand on the system. Note that in some previous studies, a cluster system was used with a RAM of up to 32 GB. Justification for simplification of the model to a closed system came as a result of the simulations taking more than a week to run on the cluster computing network. Once the model was simplified to its final closed system form, the computations typically took between 5 to 30 minutes to run.

Coupling of all three modules of Electrostatics, Transport of Diluted Species, and Laminar Flow: Once the electric field was determined to be satisfactory, the second study was run which included the coupling of all three models of Electrostatics, Transport of Diluted Species, and Laminar Flow. For the stationary solver, a relative tolerance was set at 0.001 with linearity automatically set. Linear solver Direct 1 was used for the majority of calculations; although Direct was used in some test cases. The method for termination used the nonlinear automatic newton method with an initial damping factor of 0.01, minimum damping factor of 1.0e-6, and restriction of step-size update at 10. The recovery damping factor was automatic with a recovery damping factor of 0.75. The "iterations or tolerance" termination technique was used. All solutions converged with a similar pattern.

Time-dependent model: A third simulation was used to calculate a time-dependent solution that revealed a nearly instantaneous reaction. At the start of the simulation, the analytes were even spread across the entire domain of the channel, after

which a dynamic process occurred until the reaction reached a steady state. The video produced by the simulation showed that the bulk flow of the analytes was toward the center where they concentrated and remained at seen in the final steady state solution of FIGURE 2.3c. This process was found to have a length of time between 1-2 seconds to complete.

Parameters: A preliminary study was performed in which key areas that could affect the preconcentration and detection of the analyte were identified and studied in detail; these were the voltage driving the flow, diffusivity of the analyte, permittivity, pressure point constraint, the length of the adjacent uncharged wall patches at the center of the channel, valence of the analytes, zeta potential, dimension of the channel, and concentration. All results were compared to the original model looking mostly increase of the maximum final concentration (c_{fm}) of the initial concentration (c_i); however, flow velocity profile and electric field were analyzed for completion and in some cases used to confirm the significance of certain results. Additionally, a cross-section as would connect to channels in series or parallel was explored for advancement in the area of separation and collection of the analytes. All results in the preliminary study are reported in respect to the negatively charged analyte; however, the results for the positive analyte were analyzed, with the same trends established in respect to changes in parameters. After comparing and weighing the results of the preliminary study, the conditions were optimized for instantaneous detection, measurement, and preconcentration of Cadmium.

CHAPTER 3

RESULTS

3.1 PRELIMINARY STUDY: APPLIED VOLTAGE EFFECT

The electroosmotic flow (EOF) was controlled by a voltage driven flow labeled as *V0*. It was determined that *V0* had little effect on the final concentration of the analyte, with the highest concentration being 52.466 mol/m^3 at a voltage of 6 V. Although it should be noted as the voltage approached 6 V, the electric field overtook that of the surface charge density, becoming the driving factor and causing a loss of the effect seen in original experimentation. (SEE FIGURE 3.1)

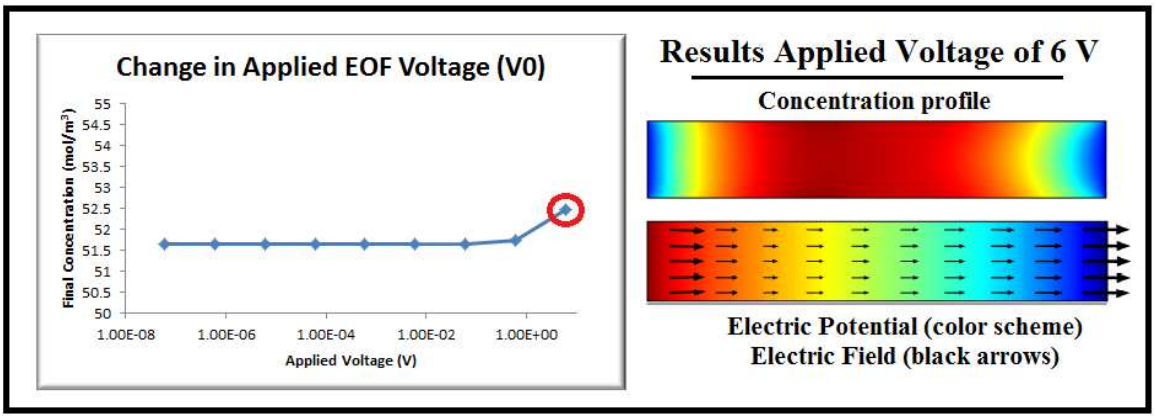

Figure 3.1 Effect of Applied Voltage: Describes the effect of changing the voltage *V0* on final concentration c_{mf}. At low V, V0 has no influence on c_{mf}. Only when voltage is significantly increased to over 1V does V affect c_{mf} (RED circle of graph on left) This effect is negated by the distortion in the concentration profile (top right) as a result of the change in electric potential where red is the highest voltage, blue is the lowest voltage, and the arrows are the magnitude and direction of the electric field (bottom right).

3.2 PRELIMINARY STUDY: EFFECT OF ZETA POTENTIAL

In micro-/nanofluidics, there is a difference in electric potential between the surface of the channel and the bulk flow at the center of the channel, which is referred to as the zeta potential. This zeta potential is caused by the spontaneous accumulation of charge at the walls which then causes charged particles to collect at the charged walls forming the EDL. For this model, the zeta potential was manipulated through changes in the surface charge density at boundaries 2, 3, 6, and 7. It was found that surface charge density is perhaps the mechanism behind the phenomenon found in this study. As zeta potential increased in magnitude via increasing the surface charge density, c_{mf} increased substantially. (SEE FIGURE 3.2) A surface charge density of -0.29 C/m^2 was the maximum condition used; increasing beyond this is a limitation of the software and was unable to compute as a result of the Debye-Hückel Approximation. This gave the largest final concentration of all tests at 1932.4 mol/m^3. Note that typical surface charge densities are on the order of -0.02 C/m^2 as was set for the initial simulation; increasing beyond this may require alteration of the surface properties.

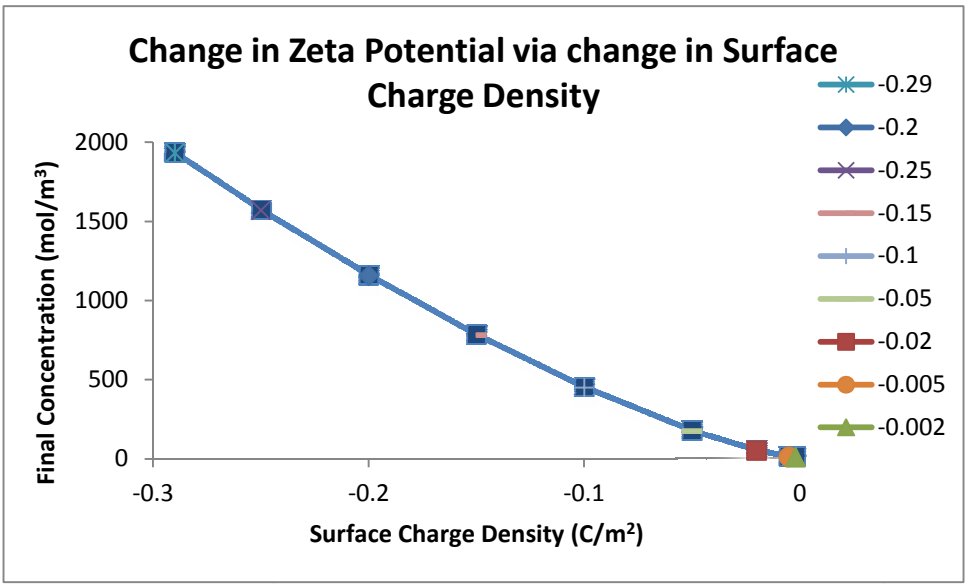

Figure 3.2 Effect of Zeta Potential: Increase in the zeta potential induced by increasing the magnitude of the surface charge density at boundary 2, 3, 6, 7 are seen to increase the maximum final concentration.

3.3 PRELIMINARY STUDY: EFFECT OF VALENCE ELECTRONS

Change in the charge, or valence, of the analytes produced some interesting and significant results which have potential to be used determine the chemical make-up of an unknown solution. Different valences ranging from +/-1 to +/-3 were tested with results seen in FIGURE 3.3 below. The highest result came with matching analyte valences of +/- 1. The second highest result doubled the original final concentration under valence of 2 and -1, which is beneficial to the final experiment with $CdCl_2$ which has the same valence.

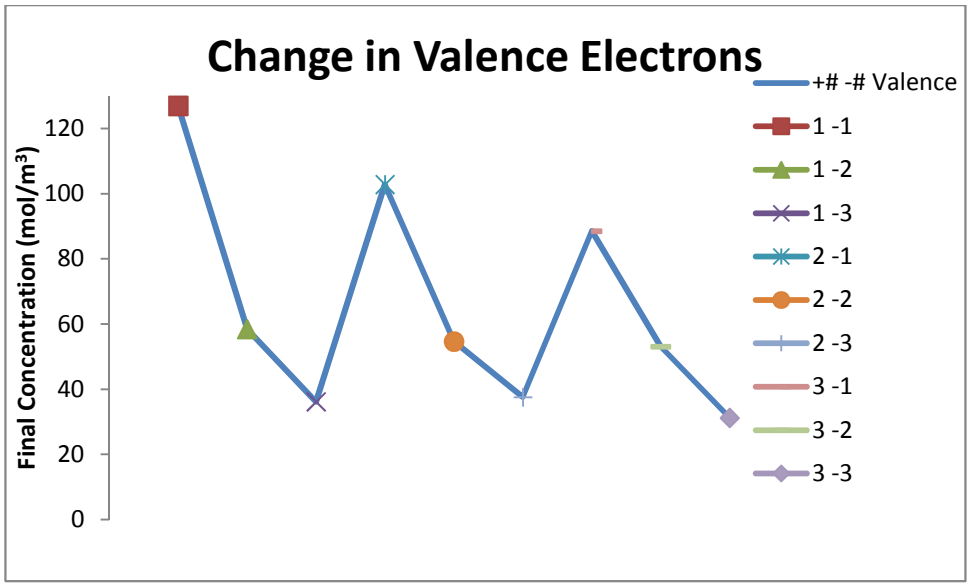

Figure 3.3 Effect of Valence Electrons: Change of the valence of the two analytes in the solution caused a change in c_{mf} with a maximum value seen in the simulation with +/-1 valence molecules (RED SQUARE) and second highest value seen in the simulation with a +2/-1 valence molecule (BLUE X with vertical line) similar to $CdCl_2$ solution and is nearly double c_{mf} of the initial model containing +/-2 valence molecules (ORANGE CIRCLE).

3.4 PRELIMINARY STUDY: UNCHARGED PATCH LENGTH EFFECT

Changing the length of the uncharged patch produced results of little significance on change in c_{mf}. As the patch length decreased, there was a slight increase in the highest final concentration calculated. With a decrease in patch length, there will also come an increase in the area coveraged by a surface charge density. This would conincidentally increase the electric field intensity in the channel, which should theoretically change the results. However, decreasing the length below the 1 um range is nearing the nanoscale and was found to lack the consolidate concentration profile important to the study. As seen in concentration profiles a channel with a 10 μm and 1 um uncharged patch length shown in FIGURE 3.4, this change in electric field caused a further consolidation of the molecules at the center of the channel. Since the EOF voltage *V0* was not altered in this

portion of the study, this finding emphasizes the importance of the role surface charge density plays in this mechanism.

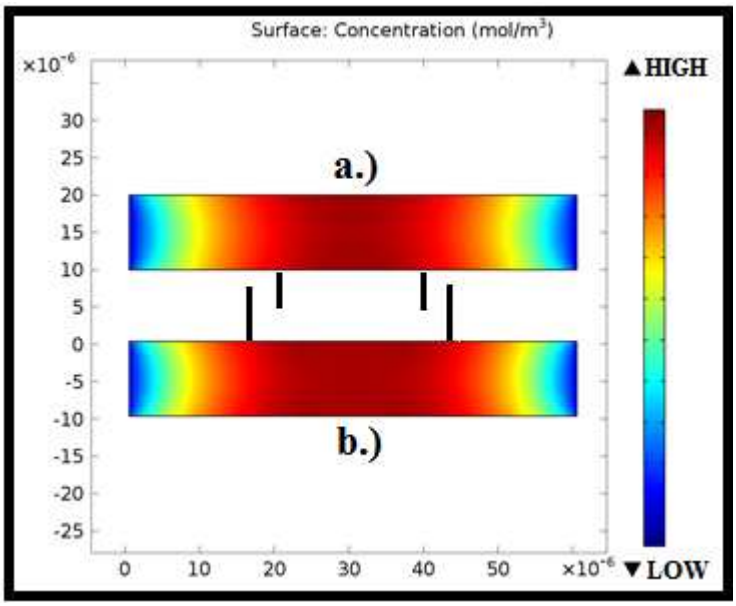

Figure 3.4 Concentration Profile Change with Uncharged Patch Length: shows the distortion of concentration profile as a result of changing the length of the uncharged wall patches, a.) 1 um patch, and b.) 10 um patch. The x-axis and y-axis represents distance in μm. A close look shows the darkest red region is smaller in a.) where the uncharged patch length is smaller.

3.5 PRELIMINARY STUDY: EFFECT OF CHANNEL DIMENSIONS

A study of the effects of the dimension of the channel was conducted in three phases; proportional change in height and width of the channel, change in height only, and change in width only; where height is used to described the distance in the y-direction and width is used to describe the distance in the x-direction. For the proportional change in dimension, the channel was both decreased and increased in size by a factor of 10. The results are seen below in FIGURE 3.5, in which the change in area as a result of changing the dimensions is compared to c_{mf}. A total of 5 simulations were run as reflected on the x-axis of FIGURE 3.5, consisting of the highest area contained in the 2-D channel of the 100x600 μm^2 (Sequence #1) and lowest area of the 0.001x0.006

μm^2 (Sequence #5). It was found that when the dimensions reached the nanoscale, the preconcentration effect was diminished. Also, when the dimensions were increased 10 fold, the preconcentration effect was nearly nonexistent. It was found that a limit was reached at the 1x6um dimension; with the highest c_{mf} of the analyte at 173.96 mol/m^3, nearly 4 times that of the initial configuration. It should be noted that at this height, the surface charge density of the channel creates the largest electric field at the center of the channel since the distance between the opposing surfaces in minimal. It was speculated that the height of the channel, which caused a variation in the electric field created by the surface charge density was the basis of this result. Further validation of this finding was completed by changing the height and width separately.

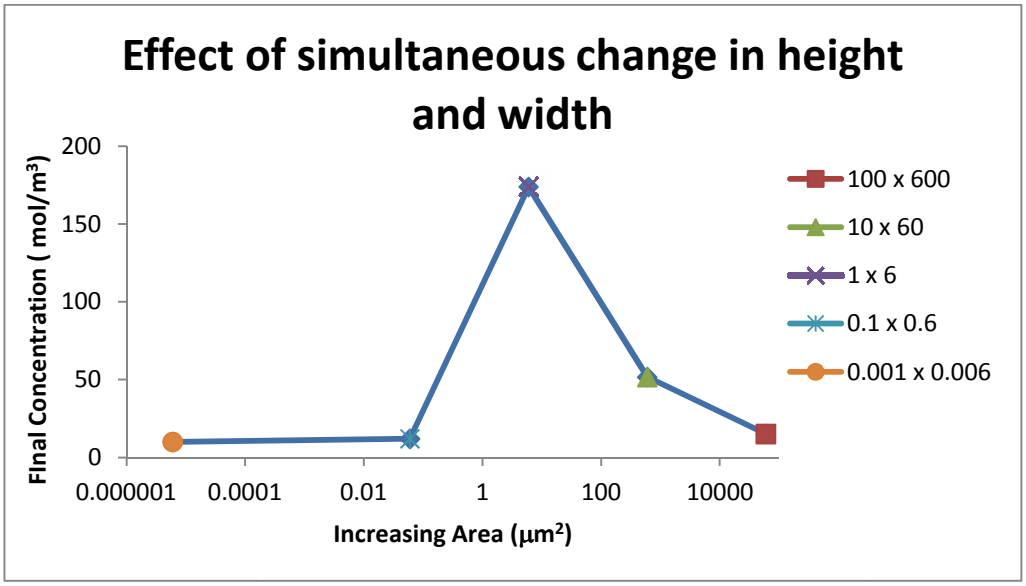

Figure 3.5 Simultaneous Change in Height and Width: Effects of changing the height and width at the same time in increments of 10. As the area contained in the channel changed, c_{mf} also changed; the highest result seen with a 1x6 um^2 channel.

It was speculated that area of the channel would affect the results; therefore the results of separately changing the height and width were compared with the change in area. (FIGURE 3.6) The results revealed that area was not the contributing factor, but

instead volume and surface charge density. In the height change study, the width was kept constant while the effects were investigated. As seen in the blue line of FIGURE 3.6, it was found that as this height decreased, thus decreasing area, c_{mf} of the analyte increased; with the highest calculated concentration being 122.1 mol/m^3 at a channel height of 5 um. Computations of a height less than 5 um were not performed. It is safe to assume that further decrease in the channel height would increase the final concentration factor as well as a continued increase in channel height causing a decrease and an eventual neglect in the preconcentration effect seen. However, the results may not remain true once the nanoscale is reached. As suggested with the proportional change in dimension, the increased preconcentration is most likely caused by the electric field created by the negative surface charge density. Throughout the study of the effects of the change in width, in order to keep a constant electric field, the voltage driving the flow was change proportionally to the change in length. As seen in the red line of FIGURE 3.6, the final concentration did go up as the length went up; with the highest calculated concentration being 159.68 mol/m^3 at a length of 300 um. Lengths beyond this began to require large amount of computational resources and were therefore halted. It can be assumed that as the final concentration would continue to increase with length. This is speculated to be in large part due to the increase in volume of the channel.

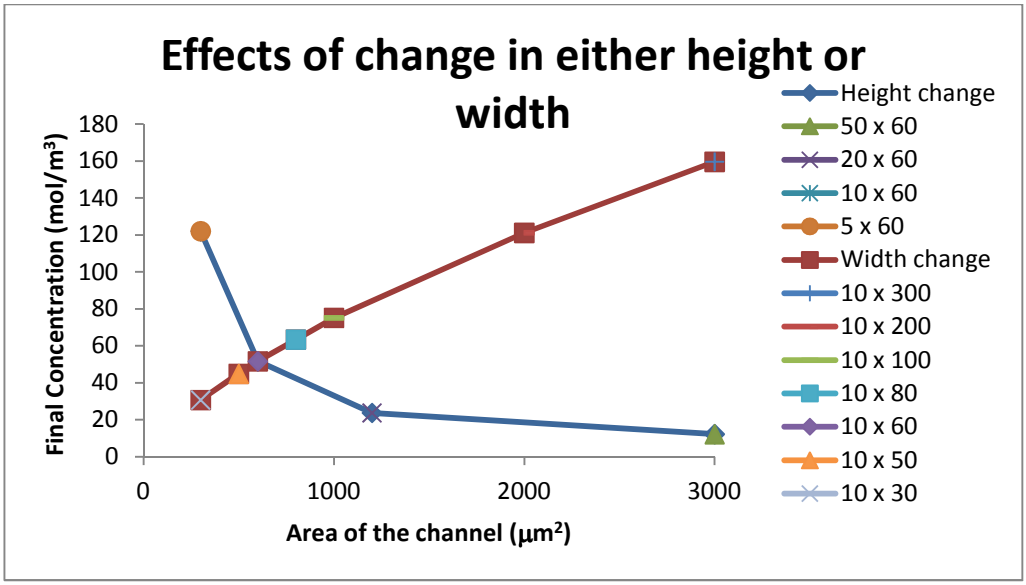

Figure 3.6 Change in Either Height or Width: Effects of changing the height and width separately, shows that as the area increases with height c_{mf} decreases (BLUE LINE) and that as the area increases with width c_{mf} increases (RED LINE).

3.6 PRELIMINARY STUDY: EFFECT OF THE INITIAL CONCENTRATION

The initial concentration of the analytes were changed in factors of 10. Seen in FIGURE 3.7, as the initial concentration increased, the final concentration increased. However, even at an increase of one factor of 10, the velocity profile of the reaction was completely different. Decreasing the concentration by factors of 10 seemed to produce a similar c_{mf} seen in the original simulation. It should be noted that the lowest initial concentration used for the simulation was 0.4 mol/m^3, which is less than half of the lowest detectable concentration limits of the current Cd detection and measurement technologies.[75-96] At the two highest concentrations of 100-1000 mol/m^3 there was almost zero change in concentration; which suggests that this phenomenon only works at lower concentrations. Comparing of the maximum final concentration divided by the initial concentration revealed an inverse relationship as seen in the bottom of FIGURE 3.7. This was to be expected and at first look may neglect the novelty of this detection

and preconcentration method; however, of note is the fact that there is zero change in the ratio of c_{mf}/c_i at the highest concentration and a large difference in the ratio at the lower concentration. This means that the mechanism found in these studies works best at lower concentrations; which coincidentally is the target of the study of detection and measurement of concentration ranges of Cd between 10-0.1 mol/m^3. Simulation of concentrations less than 0.4 mol/m^3 resulted in errors that suggest there may be a minimal concentration this mechanism can be applied for preconcentration.

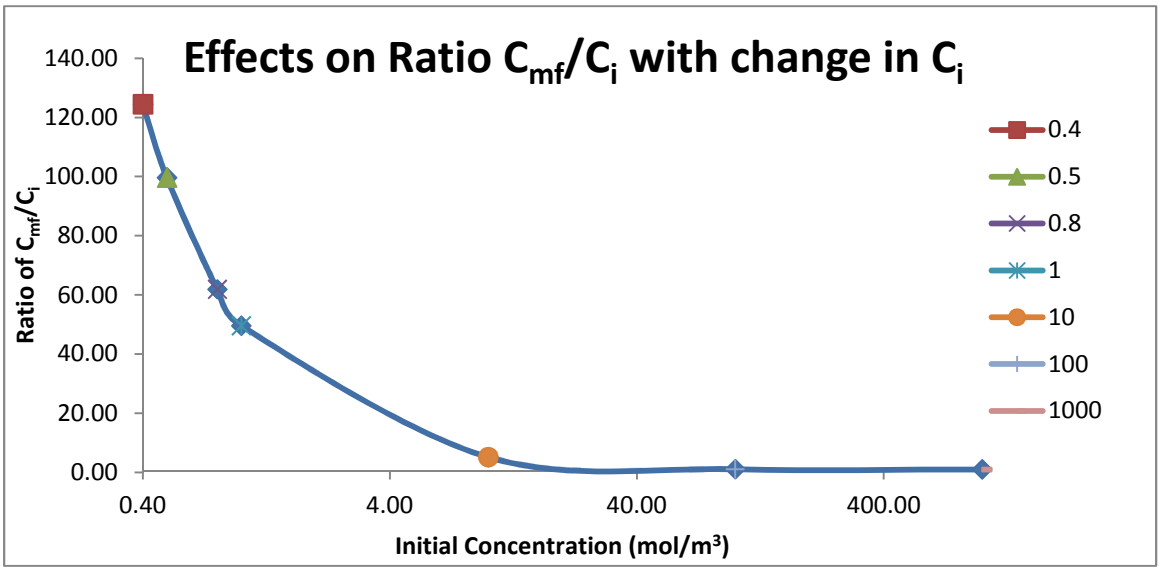

Figure 3.7 Change in Ratio of Maximum Final Concentration to Initial Concentration: Change in ratio c_{mf}/c_i as c_i is increased; Note: the lowest concentration the simulation was able to preconcentrate was 0.4 mol/m^3; the very little change in c_{mf}/c_i at high concentrations; and large differences in the ratios at lower concentrations

3.7 PRELIMINARY STUDY: EFFECT OF CROSS SECTIONAL OPENING

Since the increase in concentration between c_i and c_{mf} is relatively small in comparison to most preconcentration techniques,[104-110] a cross-section as would be seen to connect to channels in series or parallel was analyzed. The results, seen below in FIGURE 3.8, in terms of the concentration confirm that the analytes will in fact still travel to and remain at the central region of the channel where there are uncharged

surfaces. Similar to the flow velocity profile seen in FIGURE 2.3b, the flow profile represented by the black arrows shows that the general flow is to the center of the channel. However, once the molecules reach the center, it appears that the analytes would be pushed to the upper and lower sections. This is also evident by the darker red seen in the upper and lower mid-section, which indicates that this is the area with the highest concentration of analytes. Additionally, this opens the concept presented in this paper to further preconcentration by potentially connecting to other channels in series or parallel.

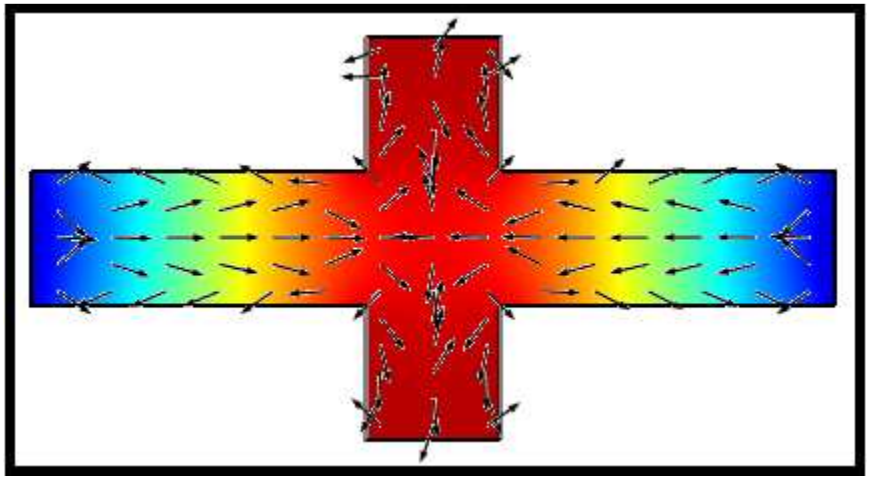

Figure 3.8 Parallel/Series Channel Cross-Section: Concentration profile of a cross-section as would connected to an adjacent channel in series or parallel; results confirmed the analytes are trapped at the center of the channel.

3.8 PRELIMINARY STUDY: EFFECT OF DIFFUSIVITY

Changing the diffusivity of the analytes had an inverse relationship; as the diffusivity decreased, the final concentration increased. Simulations were run by changing the diffusivity in factors of 10. (FIGURE 3.9) The diffusivity range of the target study of Cd detection is between 0.9-1.2 (x-9 m^2/s), which is such a small variance that the changes in diffusivity at different concentrations should not cause distinctions in

the results. Additionally, it should be noted that diffusivity can be controlled by altering the material filling the channel.

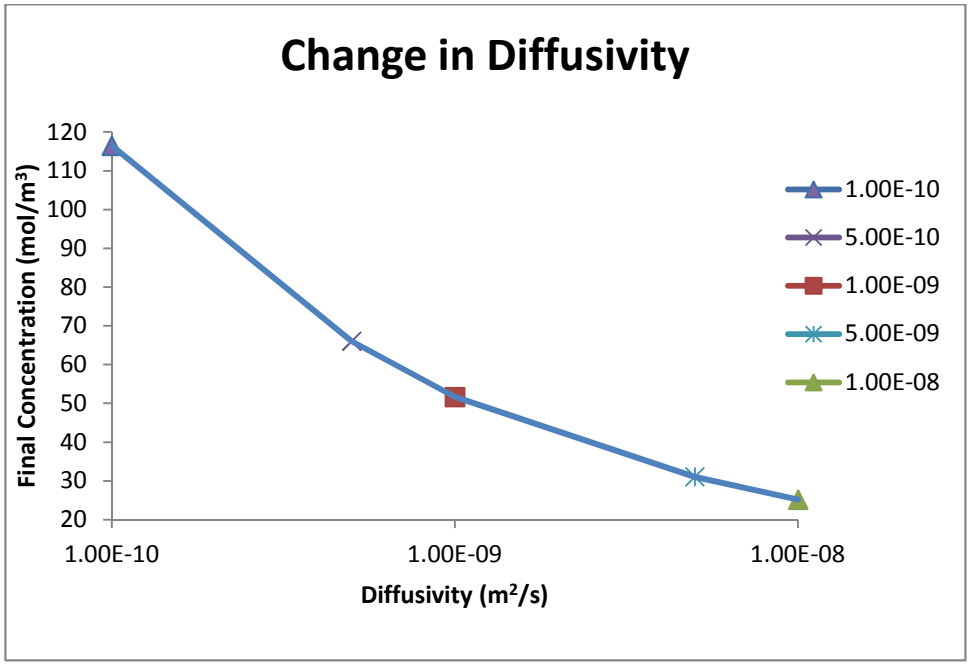

Figure 3.9 Change in Diffusivity: Changes is c_{mf} as a result of changes in the diffusivity.

3.9 PRELIMINARY STUDY: EFFECT OF PERMITTIVITY

Studies showed that permittivity has no effect on the results of the experiment, with a slight decrease as final concentration with an increase in permittivity; therefore this parameter is ignored in the final study of $CdCl_2$. (FIGURE 3.10)

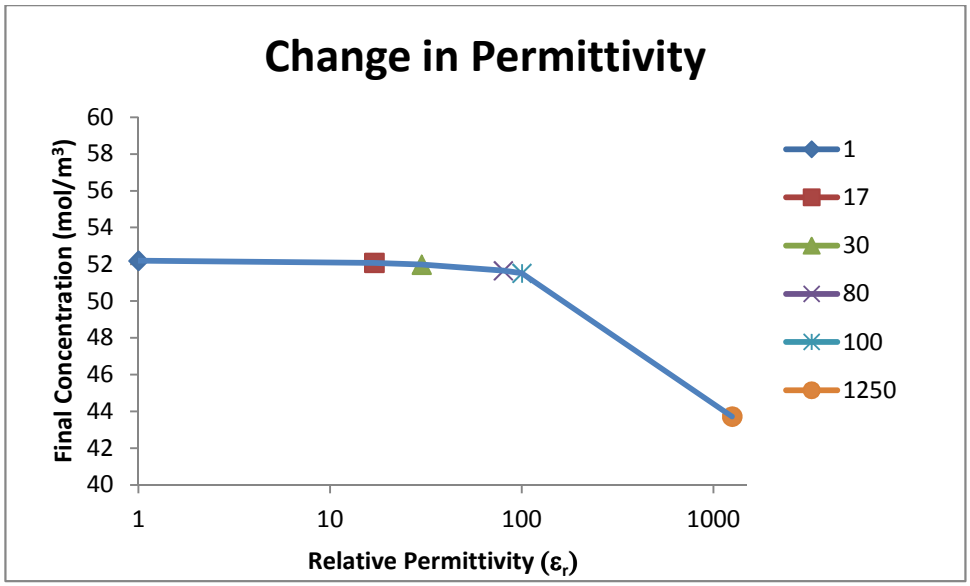

Figure 3.10 Change in Permittivity: Changes is c_{mf} as a result of changes in the permittivity. Very little change except at extremely high permittivity not seen in microfluidics.

Overall the model appears to be a valid method of preconcentration and detection with potential to determine low concentration levels instantaneously. The factors considered in this series of studies were the driven flow EOF, zeta potential, valence of the molecules in the solution, length of the charge impermeable patch, dimension of the channel, concentration, diffusivity, and permittivity. The voltage driven the EOF seemed to have little effect on the results as well as eliminating the novelty of the study at higher voltages.

3.10 OPTIMIZATION FOR CADMIUM

The first step in converting the mechanism to target the positive analyte was to study the effects on the current configuration. All results of the preliminary study showed results similar to the left column of FIGURE 3.11; in which the negative analyte had a dense population (top left) at the center and the positive analyte had a less dense concentration despite giving a larger c_{mf}. The decrease in density of the positive analyte

is most likely due to the negative surface charge densities at boundaries 2, 3, 6, and 7 (SEE FIGURE 2.4), which would attract a large number of the positive molecules. In order to overcome this, the surface charge density was charge to a positive value. These results, seen in the right column of FIGURE 3.11, reveal a reversal of positive versus negative densities at the center of the channel. Since the surface would have to undergo physical or chemical alteration to increase above a magnitude of -0.02 C/m^2, the opportunity to change the surface to a positive surface charge density is already present. Additionally, this finding confirms the influence of surface charge density over the phenomenon explored in these studies.

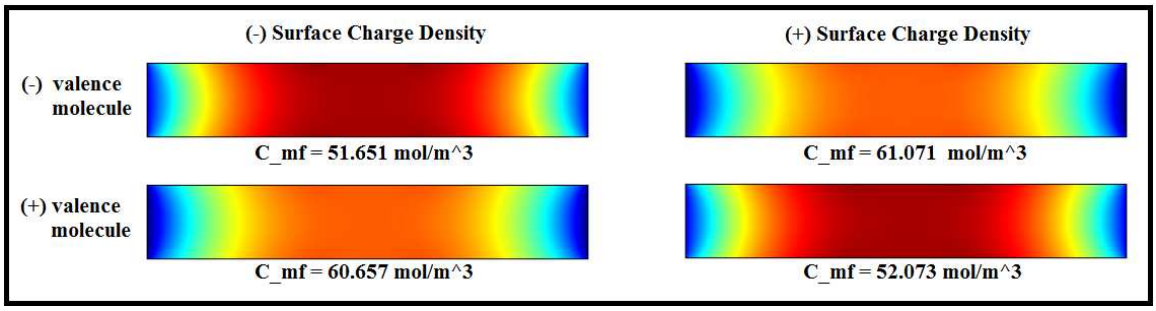

Figure 3.11 Changing Surface Charge Density to a Positive Value: Change in concentration profile as a result of changing the surface charge density from negative to positive; left column represents the profile distributions of the negative molecule (top left) and positive molecule (bottom left) in simulates with a negative surface charge density; right column represents the profile distributions of the negative molecule (top right) and positive molecule (bottom right) in simulates with a negative surface charge density.

At this point, all single-point changes in conditions were studied and believed to be understood. The preliminary studies were then used to create an optimized channel and applied to Cd preconcentration, measurement, and detection. Limitations of the software and numerical approximations based on the Debye- Hückel Approximation seemed to create a barrier for optimization. Tailoring the channel proved to not be as simple as combining the top performing conditions from each study; however, these did

help to expedite the process. The first step was to study a solution containing two molecules with a +2 and -1 valence, such as would be seen with $CdCl_2$. Since increasing the zeta potential gave the highest results over all, this served as the starting point. The surface charge density of 0.29 C/m^2, found to be the maximum value with +/-2 valence molecules, did not compute for the +2/-1 valence molecules. This is most likely due to the change in Debye Length as a result of the -1 valence versus -2 valence molecules, which is based off the Debye- Hückel Approximation used by the COMSOL software. The final optimized surface charge density determined for the study was 0.039 C/m^2. Additional problems arose when the $CdCl_2$ diffusivity values were tested, which change based on the concentration in addition to being at the lower temperature of 298 K. Temperature also seemed to complicate the simulation, but was resolved with the issues relating zeta potential. Once again, the change in valence significantly affected the computation of the results, which as previously suggested is most likely due to a change in Debye Length. Dimension change was also studied for optimization; however, there were complications with the different valence of the molecules that resulted in a decision to use the 10x60 μm^2 dimensions of the initial study. Changing the length of the channel proved to be the only option for helping to increase the final concentration; however, as stated previously, this is most likely due to the increase in volume of the channel and the decision was made to leave the dimensions in its original configuration. Final studies were performed using the initial dimension of 10x60 μm^2; additionally, this dimensional arrangement could prove to be useful in application of the technology as it is well within the range of optical measurement. Final simulations were run using a temperature of 298K and a surface charge density of -0.039 C/m^2.

Since the lowest detectable concentration of Cd using current technology is roughly 0.89 mol/m^3, it was crucial that the mechanism below this level to prove to be an improvement. Initial tests were run using the diffusivity, concentration, temperature calculated by Victo *et al.*[101] The study confirmed trends shown in the preliminary study as a result of changes in the parameters. (SEE FIGURE 3.12) In order to prove the mechanism works at levels below the current technology available, the diffusivity was calculated for a concentration of 0.5 mol/m^3 based on the values determined in the study by Victor M *et al.*[101] on the diffusivity of $CdCl_2$ at temperature of 298K. As can be seen in the top left of FIGURE 3.12, c_i ranges from 0.5 to 100 mol/m^3. Diffusivity values ranged from 1.14 ($x10^{-9}$ m^2/s) for concentration 0.5 mol/m^3 to 0.902 ($x10^{-9}$ m^2/s) for concentration 100 mol/m^3. The c_{mf} did increase with an increase in concentration. Ratio c_{mf}/c_i decreased with increasing $c_{i;}$ which additional confirmed the trend seen in preliminary experiments that the mechanism works best at lower concentrations as seen by the significant increase in the ratio c_{mf}/c_i at lower c_i.

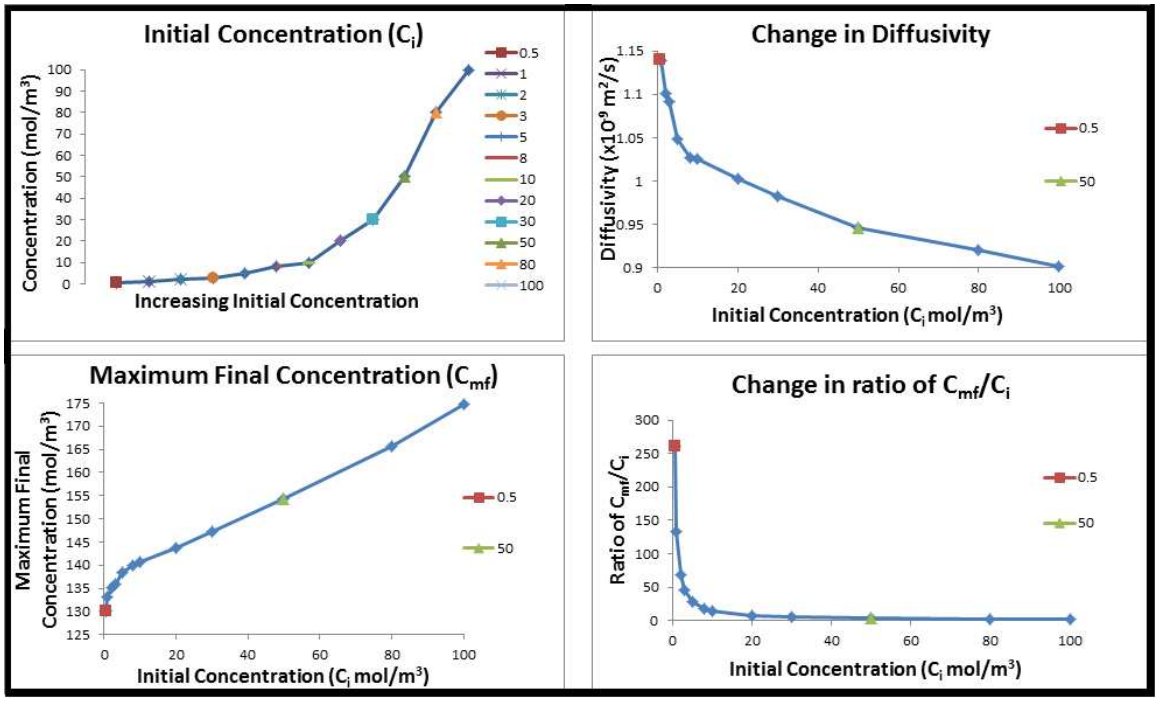

Figure 3.12 CdCl2 Graphical Response: Concentration range (top left); diffusivity range (top right); maximum final concentration (bottom left); and ratio of c_{mf}/c_i (bottom left); RED SQUARE represents the results for simulations using c_i of 0.5 mol/m^3; GREEN TRIANGLE RED SQUARE represents the results for simulations using ci of 50 mol/m^3.

It was speculated that despite the changes in diffusivity and c_{mf}, a change in concentration profile would be seen as a result of changing the initial concentration. In order to create a balanced comparison for analysis, the results for the c_i of 0.5 mol/m^3 (RED SQUARE in FIGURE 3.12) and 50 mol/m^3 (GREEN TRIANGLE in FIGURE 3.12) where observed initially. The lower diffusivity of the 0.5 mol/m^3 c_i should can only a slight increase in c_{mf} over that of the 50 mol/m^3 simulation results. This can be confirmed by the minimal increase in c_{mf} of roughly 5 mol/m^3 seen in the lower left of FIGURE 3.12. There was a significant difference in the results when observing the ratio of c_{mf}/c_i; in which the ratio was at a value of 260.14 for c_i of 0.5 mol/m^3 and only 1.7481 for c_i of 50 mol/m^3. The observed results at these concentrations gave rise to a

speculation that there would be a difference in the concentration profiles of the two simulations.

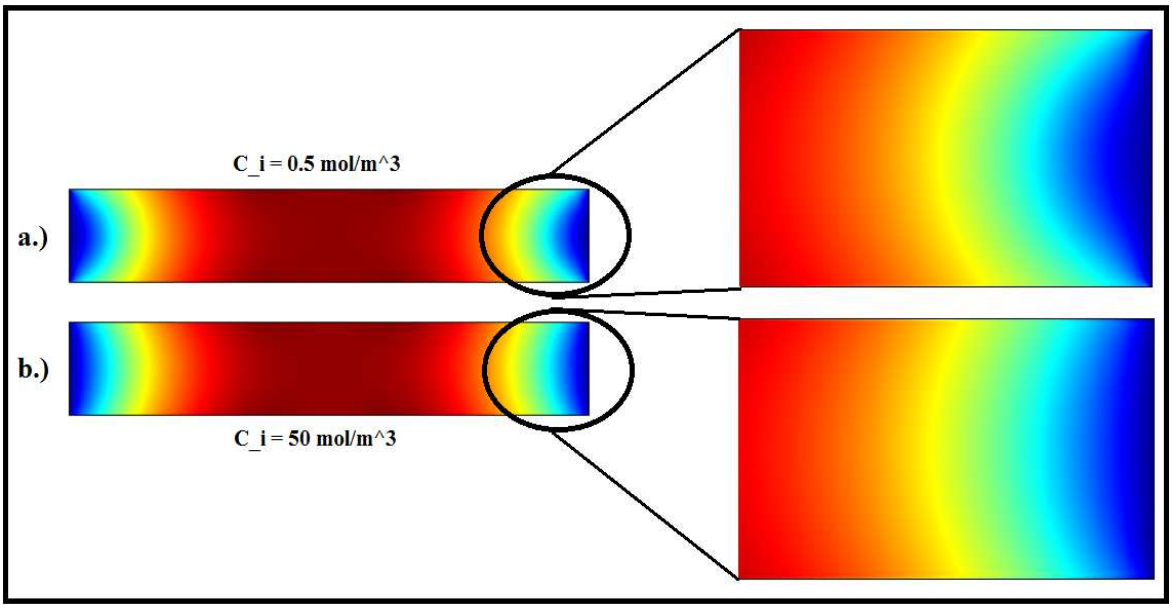

Figure 3.13 Concentration Profile Change with Initial Concentration: Comparison of the concentration profile for c_i of 0.5 mol/m^3 and 50 mol/m^3; change in distribution more clearly seen at the outer edges of the channel.

Seen in FIGURE 3.13 above, there was a difference in the concentration profile of the results which can be seen most clearly at the left and right outer edges of the channel. Despite significant effort to increase the resolution of the images, a clear distinction between the two concentration profile was not able to be seen at the center of the channel. However, the difference in concentration profile seen at the edges of the channel suggest there should be a proportional difference at the center of the channel. It is believed that given a physical model, a clear distinction would be seen between concentration profiles of the different c_i levels. Since this mechanism would be implemented by attaching a colored and/or fluorescent dye to the molecule wished to be analyzed, the final concentration profile should be clear. Finally, since the molecules were accumulated at the center of the channel for a concentration of 0.5 mol/m^3, which is nearly half the

lowest range of current technology, this mechanism is said to exceed the limits of current technology and should be explored further for implementation.

CHAPTER 4

DISCUSSION

Zeta potential, or surface charge density, was the largest contributing factor and is perhaps the mechanism driving the phenomenon. Based on a time-dependent video simulation of the model, the analytes were forced to the center of the channel; which is speculated to be a result of the negative surface charge density pulling the positive analyte to the center of the channel and constraining it there. It should be noted that micro-/nanochannels spontaneously acquire the surface charge, which is normally on the order of -0.02 C/m2. Increasing beyond this point would require alteration of the surface of the channel such as chemical or ion beam deposition. In scenarios, where the channel size is much larger than the EDL thickness (Debye length), it is computationally more reasonable to use the Smoluchowski slip velocity expression which is derived based on Poisson-Boltzmann equation & Debye-Hückel approximation. In COMSOL, Smoluchowski slip velocity (electroosmotic velocity) expression is available as wall condition; however this was not used.

Valence was also a contributing factor to final concentration. The results suggest that the composition of an arbitrary solution can be determined if other parameters, such as surface charge density, are kept constant. The fact that simulation for a solution with +2/-1 valence molecules produced such different results may be a caused by the change in Debye Length. Despite significant mesh refinement, the model was unable to perform

computations beyond the -0.029 C/m^2 surface charge density with the +2/-1 valence molecules. The errors suggest a problem in calculating the electric field gradient, which from experience is a result of a model that does not agree with theory and is therefore invalid. It is important to note that studies were performed on molecules with a singular valence meaning both positive, both negative, or one positive/negative and one with a zero valence; to which results showed a zero change in concentration, thus eliminating the effects seen in other studies. This suggests that the oppositely charged molecules are the initial driving mechanism and further implies the significance of the zeta potential on the results.

The length of the uncharged patch modeled as being impermeable to charge proved to have little in term of the significance of the final results. In fact, variation of this patch was used in the $CdCl_2$ portion of the study and created difficulty in the computation as well as having very little impact on the final to initial concentration ratio. It should also be noted, that the results are from a two-dimensional slice of a channel. These same results would perhaps be seen better by creating a three-dimensional model and varying the depth of the channel. In this model all walls of the center of the channel must remain modeled as impermeable to charge or the effects seen in this study may not apply.

The results of the dimensional change were predictable as well as significant. The electric field created by the surface charge density, which was determined to be the largest contributing factor to the experimental results, is proportional to the distance between channel walls. Therefore, the greater the distance between walls the less effect on final concentration and the less the distance between the walls the greater the effect on

the final concentration due to the change in electric field. In application, it would seem that a long channel would be most preferable as this would increase the volume within the channel and therefore increase the c_{mf}/c_i ratio. It should be noted that keeping the electric field in the x direction consistent with the experiments by proportionally changing the applied EOF voltage would be necessary to produce the desired results. Width was ignored in the final modeling of $CdCl_2$ due to its seemingly trivial nature. The final dimensions of a 10x60 μm^2 channel were studied for $CdCl_2$ due to its ease of comparison to previous experiments, as well as being within the range of optical viewing as could be seen by a person in field application.

Although the results in study as a result of change in initial concentration were predictable, as past studies as well as intuition would suggest an increase in c_{mf}/c_i ratio with a decrease in initial concentration; the result proved to be valuable. Perhaps the largest novelty found in the study is the applicability of a device that can both detect extremely low concentrations as well as predict the original concentration based on the physical profile of the analyte once voltage is applied.

Diffusivity changes as a result of temperature as well as concentration. Although in the concentration range of the $CdCl_2$ experiments, the diffusivity range was minimal, the results suggest there was little change in c_{mf}/c_i caused by diffusivity. However, based on the preliminary study, diffusivity can have a major impact on c_{mf} if the variation is large. Should diffusivity be deemed an issue, it should be noted that this value can be easily manipulated based on Einstein-Stokes equations;

$$D = \frac{k_B T}{6\pi\mu r} \tag{8}$$

where D is the diffusion, k_B is the Boltzmann constant, T is the temperature, μ is the viscosity, and r is the radius of a spherical particle. Molecules are most often modeled as spherical; therefore, since all other variables in the above equation are constant, the diffusivity can be altered by changing the viscosity of the fluid. With the ability to control the diffusivity comes the option to tailor channels to detect certain concentration ranges as well as helping to increase c_{mf}.

Changing the viscosity inside the channel would be done by changing the material, which would also change the permittivity. Since the only change in results, based on altering the permittivity of the solution, were produced by an extremely high value that would not be seen in application; there is no additional studies needed. Additionally, the basic applications of such a device as described in this study would entail combining a soil sample with water, taking a direct sample of water from a habitat, or a sample of blood/urine. In all cases, the permittivity can be modeled as that of water.

The results suggest that channels in series or parallel can used to test for increase in preconcentration effect. The simulation of a cross-section as would be seen to connect to channels in series or parallel revealed that the analytes would still gather at the central region, despite this opening. Although this did not increase the final concentration it seemed to be an option that could be applied for collection of the analytes for additional preconcentration. The analytes consolidated at this central region can then be transferred to an adjacent channel or volume via sample injection or similar mechanism. Since the ratio of c_{mf}/c_i is now known, or can be calculated by additional simulation or estimated based on the established curve; the initial concentration can be reverse calculated based

on c_{mf} and the number of channels in series or parallel. This option should be explored in detail.

In actual application of a device using the mechanism described, a fluorescent dye specific to the analyte would be mixed into solution. This would eliminate the possibility of a false positive in terms of detection. Additionally, since the simulations suggest there is a difference in concentration profile only at the edges of the channel with changing c_i, establishing a physical model is necessary to validate and confirm this change also exists at the central region of the channel that would serve to be the analysis region for detection of a specific analyte.

The presence of unknown molecules in the solution may have a direct impact on the results. This would require additional studies and simulations for determine the effect. Future studies would include studying the effect of having three or more molecules in solution. Additionally, since validation of application of the mechanism was done through targeting Cd as an analyte, other compounds other than $CdCl_2$ should be studied. Since CdO has valence charges of +/-2, parameter optimization would require minimal effort since the preliminary study included molecules with this valence. Furthermore, urine and blood samples contain relatively large concentrations of sodium chloride, which would most likely change the results an unknown amount; therefore, it is important to add a study to included NaCl in the channel solution.

Finally, a physical model would be valuable step to validation of the results seen in these simulations. Given the opportunity, these results could be reproduced and validated with relative ease. Furthermore, results of placing electrodes along the surface of the channel wall should be studied. As previously stated, the inherent electric field of

an electrode will create and electromagnetic field and should produce an electric field similar to that created by the surface charge density. Additionally, with a physical model that uses electrodes as the channel walls, the surface charge can be instantly altered and perhaps tailored to detection of specific molecules. This instantaneous alteration of surface charge would be most beneficial to the use of an open system that is reflective of the original studies that proved to be too complicated for computation.

CHAPTER 5

CONCLUSION

Cadmium detection, monitoring, and measurement are important to human health for its damage to the kidney, ecotoxicology as a result of having direct impact on physical maturation and reproduction in wild life, and radioecology due to the three naturally occurring radioactive isotopes. Due to the low sample size requirements and inexpensive nature, micro-/nanofluidics is a preferable technology for application. Above, a series of experiments is presented on the detection, preconcentration, and measurement of $CdCl_2$. This specific compound of Cadmium was chosen for its availability and solubility in water. It was initially theorized that studies would reveal a method capable of detecting Cadmium a limits lower than that of current technology. The mechanism was assumed to have the capability to detect a certain concentration based on the consolidation effect, or the trapping of the molecules at the central region of the channel. The simulations revealed that the method presented above have potential to detect Cadmium levels as low as at 0.5 mol/m^3, which is in fact less than that of current technology. It was found that the model relied upon the presence of oppositely charged valence molecules. Additionally, the overwhelming driving factor was the zeta potential created by the surface charge density. Physical models are needed to validate the computer simulations seen in these experiments; however, the results suggest that the mechanism found here can be used to further preconcentrate and measure charged molecules.

REFERENCES

1. Babich H, Stotzky G. 1977. Reductions in toxicity of cadmium to microorganisms by clay minerals. *Appl Environ Microbiol* 33:696–705.
2. Martin C, Antonini J, Doney B. 2009. A case report of elevated blood cadmium. *Occupational Med*. 59:130-132.
3. Nnorom I, Osibanjo O, Oji-Nnorom C. 2005. Cadmium determination in cigarettes available in Nigeria. *African Journal of Biotech*. 4(10):1128-1132.
4. Argonne National Laboratory. 2005. Cadmium: Human Fact Sheet.
5. Pontillon Y, Ducros G. 2010. Behaviour of fission products under severe PWR accident conditions. The VERCORS experimental programe – Part 3: Release of low-volatile fission products and actinides. *Nuclear Engineering and Design*. 240:1867-1881.
6. Chu N, Salter L, Sturniolo D. 1966. Radiochemical determination of cadmium isotopes in radioactive debris. *Talanta*. 13:283-288.
7. Bznuni S, Zhamkochyan V, Khudaverdyan A, Barashenkov, Sosnin A, Polyanski A. 2003. Cascade eletronuclear systems with a liquid-cadmium rectifier. *Atomic Energy*. 94(3):214-220.
8. Tahkur P, Balard S, Nelson R. 2012. Radioactive fallout in the United Sates due to the Fukushima nuclear plant accident. *Jof Environ Monitoring*. 14:1317-1324.
9. Nawrot T, Plusquin M, Hogervost J, Roels H, Celis H, Thijs L, Vangronsveld J, Hecke E, Staessen J. 2006. Environmental exposure to cadmium and risk of cancer: a prospective population-based study. *Lancet Oncol.* 7(2):119-126.
10. Wanger G. 1993. Accumulation of cadmium in crop plants and its consequences to human health. *Adv in Agronomy*. 51:173-212.
11. Salt D, Roger P, Pickering I, Raskin I. 1995. Mechanisms of Cadmium mobility and accumulation in indian mustard. *Plant Physiol*. 109:1427-1433.
12. Salt D, Blaylock M, Kumar N, Dushenkov V, Ensley B, Chet I, Raskin I. 1995. Phytoremediation: a novel strategy for the removal of toxic metals from the environment using plants. *Nature Biotech*. 13(5):468-474.
13. Gadd G. 1993. Interactions of fungi with toxic metals. *New Phytol*. 124:25-60.
14. Clemens S. 2001. Molecular mechanisms of plant metal tolerance and homeostasis. *Planta*. 212:475-486.

15. Schutzendubel A, Polle A. 2002. Plant responses to abiotic stresses: heavy metal-induces oxidative stress and protection by mycorrhuzation. *J of Exp Botany*. 53(372):1351-1365.

16. Sandalio L, Dalurzo H, Gomez M, Romero-Puertas M, Rio L. 2001. Cadmium-induces changes in the growth and oxidative metabolism of pea plants. *J of Exp Botany*. 52(362):2115-2126.

17. Shute T, Macfie S. 2006. Cadmium and zinc accumulation in soybean: a threat to food safety. *Sci of the Total Environ*. 371:63-73.

18. Hensbergen P, Velzen M, Nugroho R, Donker M, Straalen N. 2000. Metallothionein-bound in the gut of the insect *Orchesells cinta* (Collembola) in relation to dietary cadmium exposure. *Comp Biochem and Physiol*. 125(C):17-24.

19. Jansen M, Bruins A, Vries H, Straalen N. 1991. Comparison of cadmium kinetics in four soil arthropod species. *Arch Environ Contam Toxicol*. 20:305-312.

20. Postma J, Jong B, Staats N, Davids C. 1994. Chronic toxicity of cadmium to Chironomus riparius at different food levels. *Arch Environ.* 26:143-148.

21. Riddell D, Culp J, Baird D. 2005. Behavioral responses to sublethal cadmium exposure within an experimental aquatic food web. *Environ Toxicol and Chem*. 24(2):431-441.

22. Goto D, Wallace W. 2009. Influence of prey- and predator-dependent processes on cadmium and methylmercury trophic transfer to mumichogs. *Can J Fish Aquat Sci*. 66:836-846.

23. Ravera O. 2004. Importance and difficulties of research on metal speciation in the aquatic ecosystem: an ecologist's viewpoint. *Annali di Chimica*. 94:495-504.

24. Gross J, Johnson P, Prahl L, Karasov W. 2009. Critical period of sensitivity for effects of cadmium on frog growth and development. *Enriron Toxicol and Chem.* 28(6):1227-1232.

25. Flament S, Kuntz S, Chesnel A, Grillier-Vuissoz I, Tankazic C, Penrad-Mobayed M, Auque G, Shirali P, Schroeder H, Chardard D. 2003. Effect of cadmium on gonadognesis and metamorphosis in Pleurodeles walt. *Aquatic Toxicology*. 64:143-153.

26. James S, Little E, Semlitsch R. 2004. Effects of multiple routes of cadmium exposure on the hibernation success of the American toad. *Arch Environ Contam Toxicol*. 46:518-527.

27. James S, Little E, Semlitsch R. 2005. Metamorphosis of two amphibian species after chronic cadmium exposure in outdoor aquatic mesocosms. *Arch Environ Contam Toxicol*. 24(8):1994-2001.

28. Mouchet F, Gauthier L, Baudrimont M, Gonzalez P, Mailhes C, Ferrier V, Devaux A. 2007. Comparative evaluation of the toxicity and genotoxicity of cadmium in amphibian larvae using comet assay and the micronucleus test. *Environ Toxicol*. 22(4):422-435.

29. Fridman O, Corro L, Herkovits J. 2004. Estradiol uptake, toxicity, metabolism, and adverse effects on cadmium-treated amphibian embryos. *Environ Health Perspective*. 112(8):862-866.

30. Das S, Jana BB. 2004. Distribution pattern of ambient cadmium in wetland ponds distributed along an industrial complex. *Chemosphere.* 55:175–185.

31. Agency of Toxic Substances and Disease Registry. 1997. Toxicological Profile for Cadmium (Update). Public Health Service, U.S. Department of Health and Human Service, Atlanta, GA.

32. Gross JA, Chen TH, Karasov WH. 2007. Lethal and sublethal effects of chronic cadmium exposure on northern leopard frog (Rana pipiens) tadpoles. *Environ Toxicol Chem* 26:1192–1197.

33. James SM, Little EE. 2003. The effects of chronic cadmium exposure on American toad (Bufo americanus) tadpoles. *Environ Toxicol Chem* 22:377–380.

34. Vogiatzis AK, Loumbourdis NS. 1997. Uptake, tissue, distribution, and depuration of cadmium (Cd) in the frog Rana ridibunda. *Bull Environ Contam Toxicol* 59:770–776.

35. Godt J, Scheidig F, Grosse-Siestrup C, Esche V, Brandenburd P, Reich A, Groneberg D. 2006. The toxicity of cadmium and resulting hazards for human health. *J of Occup Med & Toxicol*. 1:22.

36. Jarup L, Berglund M, Elinder C, Nordberg G, Vahter M. 1998. Health effects of cadmium exposure: a review of the literature and a risk estimate. *Scand J Work Environ Health*. 24(1):1-51.

37. Bertin G, Averbeck D. 2006. Cadmium: cellular effect modifications of biomolecules, modulation of DNA repair and genotoxic consquences. *Biochimie*. 88:1549-1559.

38. Valle B, Ulmer D. 1972. Biochemical effect of mercury, cadmium, and lead. *Annu Rev Biochem*. 41:91-128.

39. Beyersmann D, Hechtenberg S. 1997. Cadmium, gene regulation, and cellular signaling in mammalian cells. *Toxicol Appl Pharmacol*. 144: 247–261.

40. Waisberg M, Joseph P, Hale B, Beyersmann D. 2003. Molecular and cellular mechanisms of cadmium carcinogenesis. *Toxicol*. 192: 95–117.

41. Deckert J. 2005. Cadmium toxicity in plants: is there any analogy to its carcinogenic effect in mammalian cells. *Biometals*. 18:475–481.

42. Martin C, Antonini J, Doney B. 2009. A case report of elevated blood cadmium. *Occup Med.* 59:130-132.

43. International Agency for Research on Cancer. Berrylium, cadmium, mercury and exposures in the glass manufacturing industry, in: International Agency for Research on Cancer Monographs on the Evaluation of Carcinogenic Risks to Humans. IARC Scientific Publications. Lyon. 1993:58:119–237.

44. Nnorom I, Osibanjo O, Oji-Nnorom C. 2005. Cadmium determination in cigarettes available in Nigeria. *African J of Biotech*. 4(10):1128-1132.

45. Amzal B, Julin B, Vahter M, WolkA, Johonson G, Akesson A. 2009. Population toxicokintetic modeling of cadmium for heatlh risk assessment. *Envrion Health Perspec*. 117(8):1293-1301.

46. Filipic M. 2012. Mechanisms of cadmium induced genomic instability. *Mutation Research*. 733:69-77.

47. McMurray C, Tainer J. 2003. Cancer, cadmium and genome integrity. *Nat Genet*. 34:239–241.

48. Fang M., Mar W, Cho M. 2002. Cadmium affects genes involved in growth regulation during two-stage transformation of Balb/3T3 cells. *Toxicol*. 177:253–265.

49. Yang P, Chiu S, Lin K., Lin L. 2004. Effect of cadmium on cell cycle progression in Chinese hamster ovary cells. *Chem Biol Interact*. 149:125–136.

50. Environmental Protection Agency. Technical Factsheet on: Cadmium. <http://www.epa.gov/ogwdw/pdfs/factsheets/ioc/tech/cadmium.pdf>. Visited July 2012.

51. Environmental Protection Agency. Consumer Factsheet on: Cadmium. <http://www.epa.gov/ogwdw/pdfs/ factsheets/ioc/cadmium.pdf>. Visited in July 2012.

52. Environmental Protection Agency. Cadmium. CAS Number: 7440-43-9. <http://www.epa.gov/osw/hazard/ wastemin/minimize/factshts/cadmium.pdf>. Visited in July 2012.

53. Occupational Safety & Health Administration. Cadmium. <http://www.osha.gov/SLTC/cadmium/index .html>. Visited in July 2012.

54. Occupational Safety & Health Administration. Cadmium. <http://www.osha.gov/Publications/osha3136. pdf>. Visited in July 2012.

55. Occupational Safety & Health Administration. OSHA 3136-08R. Cadmium. <http://www.osha.gov/ Publications/3136-08R-2003-English.html>. Visited in July 2012.

56. Occupational Safety & Health Administration. Toxic Hazardous Substances. 1910.1027. Cadmium. <http:// www.osha.gov/pls/oshaweb/owadisp.show_document?p_table=standards&p_id=10035>. Visited in July 2012.

57. Ikechukwu E, Ajeh E. 2011. Histopathological Alterations in the liver and lungs of Hoplobatrachis occipitalis exposed to sub lethal concentration of cadmium. *Australian J of Basic & App Sci*. 5(11):1062-1068.

58. Friberg L, Kjellstrom T, Nordberg G. Cadmium, in: L. Friberg, G.F. Nordberg, V.B. Voul (Eds.), Handbook on the Toxicology of Metals, second ed, Elsevier, Oxford, 1986, pp. 130–184.

59. Kasuya M, Teranishi H, Aoshima K, Katoh T, Horiguchi H, Morikawa Y, Nishijo M, Iwata K. 2000. Water pollution by cadmium and the onset of Itai–itai disease. *Water Sci. Technol*. 25:149–156.

60. Geoffroy-Siraudin C, Perrard M, Ghalamoun-Slaimi R, Ali S, Chaspoul F, Lanteaume A, Achard V, Gallice P, Durand P, Guichaoua M. 2012. Ex-vivo assessment of chronic toxicity of low levels of cadmium on testicular meiotic cells. *Toxicol & App Pharm*. 262:238-246.

61. International Agency for Research on Cancer. Berrylium, cadmium, mercury and exposures in the glass manufacturing industry, in: International Agency for Research on Cancer Monographs on the Evaluation of Carcinogenic Risks to Humans, vol. 58, IARC Scientific Publications, Lyon, 1993, pp. 119–237.

62. Jin T, Kong Q, Ye T, Wu X, Nordberg G. 2004. Renal dysfunction of cadmium-exposed workers residing in a cadmium-polluted environment. *Biometals*. 17:513–518.

63. Schneider M, Sullivan J, Wach P, Boesen E, Fukai T, Pollock J, Pollock D. 2010. Protective role of extracellular superoxide dismutase in renal ischemia/reperfusion injury. *Kidney International*. 78(4):374-81.

64. Schneider P, Wach P, Durley M, Pollock J, Pollock D. 2010. Sex difference in acute angiotensin II-mediated hemodynamic response in mice. *American J of Physiology*. 299(3):R899-906.

65. Adams R, Harrison J, Scott P. 2012. The development of cadmium-induced proteinuria, impaired renal function, and osteomalacia in alkaline battery workers. *Oxford J of Med*. 38(4):425-443.

66. Potts C. 1965. Cadmium proteinuria. *Ann Occup Hyg*. 8:55-61.

67. Nordberg G. 1972. Cadmium metabolism and toxicity experimental studies on mice with special reference to the use of biological materials as indices of retention and the possible role of metallothionein in transport and detoxification of cadmium. *Environ Physiol Biochem*. 2:7-36.

68. Nordberg M, Nordberg G, Piscator M. Isolation and characterization of a hepatic metallothionein from mice. Environ Physiol Biochem 1975;5(6):396–403.

69. Nordberg G, Nogawa K, Nordberg M, Friberg L. Cadmium. In: Nordberg, et al., editors. Handbook on the toxicology of metals. 3rd ed. Academic Press/Elsevier; 2007. p. 446–86 [chapter 23].

70. Nordberg M, Nordberg G. 2000. Toxicological aspects of metallothionein. *Cell Mol Biol*. 46(2):451-63.

71. Hildebrand CE, Cram LS. 1979. Distribution of cadmium in human blood cultured in low levels of CdCl2. *Proc Soc Exp Biol Med*. 161:438–43.

72. Nordberg GF. 2009. Historical perspectives on cadmium toxicology. *Toxicol Appl Pharmacol.* 238:192-200.

73. Lauwerys R, Bernard A, Roels H, Buchet J. 1994. Cadmium: exposure markers as predictors of nephrotoxic effects. *Clin Chem*. 40(7):1391-1394.

74. Chang C, Lauwerys R, Bernard A, Roels H, Buchet J, Garvey J. 1980. Metallothionein in Cadmium-exposed workers. *Eviron Research*. 23:422-428.

75. International Programme on Chemical Safety. Environmental Health Criteria 134, Cadmium. <http://www. inchem.org/documents/ehc/ehc/ehc134.htm>. Visited in July 2012.

76. Jahromi E, Bidari A, Assadi Y, Hoseini M, Jamali M. 2007. Dispersiv liwuid-liquid microextraction combined with graphite furnace atomic absorption spectrometry ultra trace determination of cadmium in water samples. *Analytica Chimica Acta*. 585:305-311.

77. Sperling M, Yin X, Welz B. 1991. Flow injection on-line separation and preconcentration of electrothermal atomic absorption spectrometry. *J of Anal Atomic Spec.* 6:295-300.

78. Fang Z, Xu S, Dong L, Li W. 1994. Determination of cadmium in biological materials by flame atomic absorption spectrometry with flow-injection on-line sorption preconcentration. *Talanta*. 41(12):2165-2172.

79. Manzoori J, Bavili-Tabrizi A. 2002. Cloud point preconcentration and flame atomic absorption spectrometric determination of Cd and Pb in human hair. *Analytica Chimica Acta*. 470:215-221.

80. Pharr K, Jones B. 2007. Extraction of cadmium from urine: a brief review. *App Spec Reviews*. 42:563-572.

81. Delves H. 1982. Analytical techniques for measuring cadmium in blood. In: Proceedings of the International Workshop on Biological Indicators on Cadmium Exposure Diagnostic and Analytical Reliability. *Commission of the European Communities*. 1-15.

82. Piscator M, Friberg L, Nordberg G. 1971. Data on interferences in cadmium analysis. ed Cadmium in the environment, Cleveland, Ohio, CRC Press, p 17.

83. Jagner D, Josefson M, Westerlund S. 1981. Simultaneous determination of cadmium and lead in urine by means of computerized potentiometric stripping analysis. *Anal. Chim. Acta.* 128:155-161.

84. Halvorsen C, Steinnes E. 1975. Simple and precise determination of Zn and Cd in human liver by neutron activation analysis. Z *Anal Chem*. 274:199-202.

85. Kjellstrom T, Tsuchiya K, Tompkins E, Takabatake E, Lind B, Linnman L. 1975. A comparison of methods for analysis of cadmium in food and biological material. A cooperative study between Sweden, Japan, and the USA. In: Recent advances in the assessment of the health effects of environmental pollution, Luxembourg, Commission of the European Communities, pp. 2197-2213.

86. Kjellstrom T. 1979. Exposure and accumulation of cadmium in populations from Japan, the United States, and Sweden. *Environ Health Perspect.* 28:169-197.

87. Jawaid M, Lind B, Elinder C. 1983 Determination of cadmium in urine by extraction and flameless atomic absorption spectrophotometry. Comparison of urine from smokers and non-smokers of different sex and age. *Talanta*. 30:509-513.

88. Biggin H, Chen N, Ettinger Km Fremlin J, Morgan W, Nowotny R, Chamberlain M, Harbey T. 1974. Cadmium by in vivo neutron activation analysis. *J Radioanal Chem*. 19:207-214.

89. Harvery T, McLellan J, Thomas B, Fremlin J. 1975. Measurement of liver cadmium concentrations in patients and industrial workers by neutron activation analysis. *Lancet*. 1:1269-1272.

90. McLellan J, Thomas B, Fremlin J. 1975. Cadmium: its in vivo detection in man. *Phys Med Biol*. 20:88-95.

91. Thomas B, Harvery T, Chettle D, McLellan J, Fremlin J. 1979. A transportable system for the measurement of liver cadmium in vivo. *Phys Med Biol*. 24:432-437.

92. Ellis K, Morgan W, Zanzi I, Yasumura S, Vartsky D, Cohn S. 1981. Critical concentrations of cadmium in human renal cortex: dose-effect studies in cadmium smelter workers. J of Toxicol Environ Health. 7:691-703.

93. Al-Haddad I, Chettle D, Fletcher J, Fremlin J. 1981. A transportable system for measurement of kidney cadmium in vivo. *Int J of Appl Radiat. Isot*. 32:109-112.

94. Ahlgren L, Mattson S. 1981. Cadmium in man measured in vivo by X-ray fluorescence analysis. *Phys Med Biol*. 26:19-26.

95. Christofferson J, Mattson S. 1983. Polarized X-rays in XRF-analysis for improved in vivo detectability of cadmium in man. *Phys Med Biol*. 28:1135-1144.

96. Skerfving S, Christofferson J, Shutz A, WElinder H, Spang G, Ahlgren L, Mattson S. 1987. Biological monitoring, by in vivo XRF measurements, of occupational exposure to lead, cadmium and mercury. *Biol Trace Elem Res*. 13:241-251.

97. Han J, Craighead H. 2000. Separation of long DNA molecules in a microfabricated entropic trap array. *Science*. 288(5468):1026-1029.

98. Nissenson A. 2009. Bottom-up nanotechnology: the human nephron filter. *Semin Dial*. 22(6):661-4.

99. Stein D, Kruithof M, and Dekker C. 2004. Surface-charges-governed ion transport in nanofluidic channels. *Phys Rev Let*. 93(3):035901(1-4).

100. Wang Y, Pant K, Chen Z, Wang G, Diffey W, Ashley P, Sundaram S. 2009. Numerical analysis of electrokinetic transport in micro-nanofluidic interconnect preconcentration in hydrodynamic flow. *Microfluid Nanofluid*. 7(5):683-696.

101. Victor M, Lobo M, Quaresma JL. 1990. Diffusion coefficients in aqueqous solutions of cadmium chloride at 298 K. *Electrochmicia Acta*. 35(9):1433-1436.

102. Kirby B. 2010. Micro- and Nanoscale Fluid Mechanics: Transport in Microfluidic Devices: *Cambridge University Press*.

103. Groisman, A, Steinberg V. 2001. Efficient mixing at low Reynolds numbers using polymer additives. *Nature*. 410:905-908.

104. Lin C, Hsu J, Lee G. 2011. Sample preconcentration in microfluidic devices. Microfluid Nanofluid. 10:481-511.

105. Kenyon S, Melghan M, Hayes M. 2011. Review: Recent development in electrophoretic separations in microfluidic devices. Electrophoresis. 32:482-493.

106. Zangle T, Mani A, Santiago J. 2010. Theory and experiments of concentration polarization and ion focusing at microchannel and nanochannel interfaces. Chem Soc Rev. 39:1014-1035.

107. Bruin G. 2000. Review: recent development in electrokinetically driven analysis on microfabricated devices. Electrophoresis. 21:3931-3951.

108. Svec F. 2006. Less common applications of monoliths: preconcentration and solid-phase extraction. Chromatography. 841:52-64.

109. Park S, Chung T, Kim H. 2009. Ion bridges in microfluidic systems.. Microfluid Nanofluid. 6:315-331.

110. Holtzel A, Tallarek U. 2007. Review: ionic conductance of nanopores in microscale analysis systems. J Sep Sci. 30:1398-1419.

111. Gonsalves P. The design and fabrication of microfluidic reactor for synthesis of cadmium selenide quantum dots using silicon and glass substrates. *Thesis: California Polytechnic State University*. 27 February 2012.

112. Mahto S, Yoon T, Shin H, Rhee S. 2009. Multicompartmented microfluidic device for characterization of dose-dependent cadmium cytotoxicity in BALB/3T3 fibroblast cells. *Biomed Microdevices*. 11(2):401-411.

113. Zhang H, Faye D, Lefevre J, Delaire J, Leray I. 2013. Selective fluorimetric detection of cadmium in a microfluidic device. *Microchem*. 106:167-173.